AUBURN UNIVERSITY
Samuel Ginn College of Engineering

Final Report for ALDOT Project 930-988

CHARACTERIZING STRENGTH LOSS IN HIGH PLASTICITY CLAYS ALONG ALABAMA HIGHWAYS

Submitted to

The Alabama Department of Transportation

Prepared by

Mengwei Xuan
Jack Montgomery
J. Brian Anderson
Michael Kiernan

March 2023

Highway Research Center
Harbert Engineering Center
Auburn, Alabama 36849

www.eng.auburn.edu/research/centers/hrc.html

1. Report No. 930-988	**2. Government Accession No.**	**3. Recipient Catalog No.**
4. Title and Subtitle Characterizing Strength Loss in High Plasticity Clays Along Alabama Highways		**5. Report Date** March 2023
		6. Performing Organization Code
7. Author(s) Mengwei Xuan, Jack Montgomery, J. Brian Anderson, Michael Kiernan		**8. Performing Organization Report No.** 930-988
9. Performing Organization Name and Address Highway Research Center Department of Civil Engineering 238 Harbert Engineering Center Auburn, AL 36849		**10. Work Unit No. (TRAIS)**
		11. Contract or Grant No.
12. Sponsoring Agency Name and Address Alabama Department of Transportation 1409 Coliseum Boulevard Montgomery, AL 36130-3050		**13. Type of Report and Period Covered** Technical Report
		14. Sponsoring Agency Code

15. Supplementary Notes
Project performed in cooperation with the Alabama Department of Transportation.

16. Abstract

Strength loss in high plasticity clay soils is a common occurrence along roadways in western and central Alabama and has considerable impact on pavement distress and slope failures. Approximately $16 million was spent to repair slope failures in western and central Alabama between 2005 and 2015 with many of these failures occurring in areas with high plasticity Prairie clays. Selecting strengths for these soils to use in slope stability analyses is often a key source of uncertainty and the selected strengths must account for effects of loading conditions and any potential changes in strength over time. For high plasticity clay, such as the Prairie clays in Alabama, repeated cycles of wetting and drying can reduce the available drained shear strength to the fully softened condition before large movements occur. This reduction in strength can lead to failure without any change in loading and accounting for this potential strength loss when analyzing the stability of these slopes is critical to obtain accurate results. The torsional ring shear test can measure both the fully softened strength (used for first time failures) and the residual strength (used for ongoing or reactivated failures) of high plasticity clays. For this study, clay samples were collected at six landslide sites around Alabama. Samples were tested to determine the index properties, electrical resistivity, mineralogy, and fully softened and residual strengths. The results from these tests were compared with existing correlations to determine which correlations were the most appropriate for use in Alabama. For three of the sites, slope stability analyses were performed to compare with observed performance at the site. The results show that the strength envelopes from ring shear testing are consistent with the observations at all three sites, although nonlinear envelopes are needed for some sites. Recommendations are provided for correlations that can be used to estimate strengths when ring shear testing is not available and for cases where existing correlations do not provide good estimates.

17. Key Words Torsional ring shear; High plasticity clay; Drained shear strength; Slope stability; Nonlinear strength envelopes		**18. Distribution Statement** No restrictions.	
19. Security Classification (of this report) Unclassified	**20. Security Classification (of this page)** Unclassified	**21. No. of Pages** 81	**22. Price** None.

Research Report

CHARACTERIZING STRENGTH LOSS IN HIGH PLASTICITY CLAYS ALONG ALABAMA HIGHWAYS

Submitted to

The Alabama Department of Transportation

Prepared by

Mengwei Xuan

Jack Montgomery

J. Brian Anderson

Michael Kiernan

March 2023

DISCLAIMERS

The contents of this report reflect the views of the authors who are responsible for the facts and accuracy of the data presented herein. The contents do not necessarily reflect the official views or policies of the Alabama Department of Transportation, Auburn University, or the Highway Research Center. This report does not constitute a standard, specification, or regulation. Comments contained in this report related to specific testing equipment and materials should not be considered an endorsement of any commercial product or service; no such endorsement is intended or implied.

NOT INTENDED FOR CONSTRUCTION, BIDDING, OR PERMIT PURPOSES

Jack Montgomery, Ph.D.

Research Supervisor

ACKNOWLEDGEMENTS

Material contained herein was obtained in connection with a research project, "Characterizing Strength Loss in Prairie Clays Along Alabama Highways," ALDOT Project 930-988, conducted by the Auburn University Highway Research Center. Funding for the project was provided by the Alabama Department of Transportation (ALDOT). The funding, cooperation, and assistance of many individuals from each of these organizations are gratefully acknowledged. The authors particularly acknowledge the contributions of the following individuals for serving on the project advisory committee and assisting with the data collection and processing:

Scott George	ALDOT, Materials and Test Engineer, Montgomery
Kaye Chancellor Davis	ALDOT, Deputy State Materials and Tests Engineer, Montgomery
Shannon Golden	ALDOT, State Maintenance Engineer, Montgomery
Skip Powe	ALDOT, State Construction Engineer, Montgomery
Virgil Clifton	ALDOT, Research and Development Bureau, Montgomery
Calvin Smith	ALDOT, Research and Development Bureau, Montgomery
Kristy Harris	FHWA
Brannon McDonald	ALDOT, Materials and Tests Bureau, Montgomery
Renardo Dorsey	ALDOT, Materials and Tests Bureau, Montgomery
Victor Aguilar	Auburn University (former student)
Patricia Carcamo	Auburn University (former student)
Dan Jackson	Auburn University (former student)

ABSTRACT

Strength loss in high plasticity clay soils is a common occurrence along roadways in western and central Alabama and has considerable impact on pavement distress and slope failures. Approximately $16 million was spent to repair slope failures in western and central Alabama between 2005 and 2015 with many of these failures occurring in areas with high plasticity Prairie clays. Selecting strengths for these soils to use in slope stability analyses is often a key source of uncertainty and the selected strengths must account for effects of loading conditions and any potential changes in strength over time. For high plasticity clay, such as the Prairie clays in Alabama, repeated cycles of wetting and drying can reduce the available drained shear strength to the fully softened condition before large movements occur. This reduction in strength can lead to failure without any change in loading and accounting for this potential strength loss when analyzing the stability of these slopes is critical to obtain accurate results. The torsional ring shear test can measure both the fully softened strength (used for first time failures) and the residual strength (used for ongoing or reactivated failures) of high plasticity clays. For this study, clay samples were collected at six landslide sites around Alabama. Samples were tested to determine the index properties, electrical resistivity, mineralogy, and fully softened and residual strengths. The results from these tests were compared with existing correlations to determine which correlations were the most appropriate for use in Alabama. For three of the sites, slope stability analyses were performed to compare with observed performance at the site. The results show that the strength envelopes from ring shear testing are consistent with the observations at all three sites, although nonlinear envelopes are needed for some sites. Recommendations are provided for correlations that can be used to estimate strengths when ring shear testing is not available and for cases where existing correlations do not provide good estimates.

TABLE OF CONTENTS

List of Tables

List of Figures

CHAPTER 1: INTRODUCTION

1.1 Background

Shallow slope failures are a common occurrence in both fill and cut slopes in western Alabama. In this area and others, expansive clays in the Selma, Tuscaloosa, and Midway Groups (Figure 1-1), sometimes referred to as Prairie clays, exhibit very low strengths causing repeated failures of even relatively flat slopes. Failures in geologic units with Prairie clays cost the state of Alabama a significant amount of money each year. The Alabama landslide database (Knights et al. 2020) found that almost $16 million was spent to repair slope failures in the Selma, Tuscaloosa and Midway Groups between 2005 and 2015. This figure only includes landslides for which federal emergency relief funds were requested, so the repair cost for all landslides in these units is likely much higher. This figure also does not include maintenance costs needed to repave and regrade shoulder failures (Stallings 2016). It is believed that these failures are at least partially due to strength loss following repeated cycles of wetting and drying in the high plasticity clays that are ubiquitous in these regions. This reduction in strength can lead to failure without any change in loading (Khan et al. 2017). Understanding the strength of these soils is critical to be able to design effective repairs and avoid repeated failures.

Soil strengths for slope stability studies are commonly estimated using triaxial tests on undisturbed or remolded samples, but while these tests can be used to measure the fully softened strength (i.e., the peak drained shear strength of a clay soil under normally consolidated conditions), they cannot reach large enough shear strains to accurately determine the residual strength (Skempton 1970). In overconsolidated clays, softening tends to occur quickly after reaching the peak strength (Holtz et al. 2011), therefore, residual strengths can be an important factor in measuring the stability of overconsolidated clay slopes (Skempton 1970, 1984, 1985). The ring shear test (Bromhead 1979, ASTM D6467, Stark and Vettel 1992) can be used to measure residual strengths of clays, but its use in practice is still limited due to limited availability of the equipment in commercial labs and the difficulty in preparing high quality specimens. To overcome some of the difficulties in both the laboratory and field measurements of fully softened strengths, correlations have been developed which relate the long-term strength of the clay to an index property such as the Atterberg Limits (e.g., Stark and Eid 1994, 1997, Mesri and Shahien 2003, Stark and Hussain 2013, Eid and Rabie 2017, Stark and Fernandez 2020), which is commonly

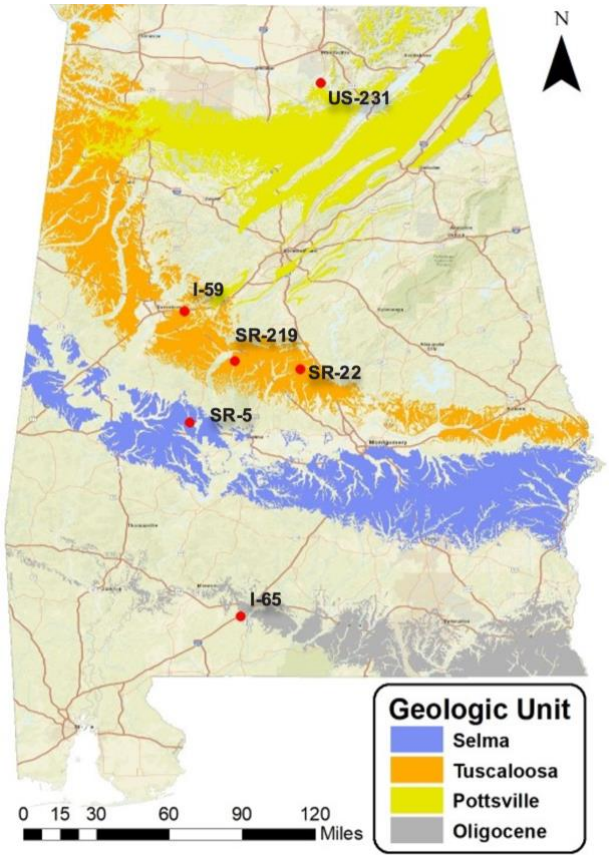

Figure 1-1: Locations of sites and key geologic units (after Szabo et al. 1988).

measured during routine geotechnical investigations. These correlations depend on the properties and mineralogy of the clay deposit, so correlations must be developed or verified for use in regions where these materials are found. Previous authors have also highlighted the importance of considering nonlinear strength envelopes for both fully softened and residual strengths (Stark and Eid 1997, Mesri and Shahien 2003, and Lade 2010), although the use of these envelopes is still limited in practice.

The objective of this study was to develop strength envelopes for clay samples collected at six landslide sites (Figure 1-1) and compare those strength envelopes to existing correlations for fully softened and residual strengths. The samples were characterized to determine index properties (Atterberg limits and clay fraction), electrical resistivity (field and/or lab tests), and mineralogy through X-ray diffraction. Ring shear testing was performed on each of the samples to measure the fully softened and residual strength envelopes over a wide range of stresses. These strength results were then compared with predictions from existing correlations for both fully softened and residual strengths (Mesri and Shahien 2003, Wright 2005, Stark and Hussain 2013,

Eid et al. 2016, Eid and Rabie 2017, and Stark and Fernandez 2020) to determine how well existing correlations fit the measured data. The developed strength envelopes were also used to perform slope stability analyses for three of the sites, which demonstrated that the measured strength envelopes can match the observed performance. The importance of using nonlinear envelopes for these sites was also explored.

The findings from this work highlight the importance of considering potential for strength loss when analyzing landslides in high plasticity clays. Ring shear testing is a good way to measure these strengths, but the tests are rather slow and the equipment is not commonly available in commercial laboratories. The correlations developed by Mesri and Shahien (2003) and Stark and Hussain (2013) show reasonable agreement with the measured strengths from most of the sites and can be used to estimate strengths when ring shear testing is not available. The exception to this is the residual strengths measured for the clay at the Laceys Spring landslide on US-231. This soil shows a very nonlinear residual strength envelope that cannot be easily fit with any of the existing correlations. The findings from this study can be used to help improve current procedures to estimate strengths of clayey soils for use in slope stability analyses and provide more reliable estimates of stability and more effective designs for repairs. Recommendations for implementing this research into current ALDOT practice are discussed. Topics related to this study that could benefit from future research are also discussed.

1.2 Project Objectives

The overall purpose of this research was to develop approaches to estimate the potential for strength loss in clays in Alabama and provide guidance on the use of these strengths in slope stability analyses. This was accomplished through field and laboratory testing of soils at several landslide sites (Figure 1-1) to determine fully softened and residual strength envelopes and correlate these envelopes with more commonly measured soil properties. Specific objectives for this project include:

1. Collect detailed information on laboratory test procedures and existing correlations for the fully softened and residual strengths of materials similar to Prairie clays.
2. Perform in-situ tests at landslide sites with Prairie clays, along with sampling for laboratory tests.
3. Characterize the collected samples and conduct ring shear tests on the clay specimens in the laboratory.

4. Evaluate correlations between the fully softened strength and index properties for clays in Alabama.
5. Develop guidance for ALDOT engineers on the measurement and use of fully softened and residual strengths in geotechnical design.

1.3 Scope of Work

The following tasks were performed to accomplish the research objectives of this project:

- Task 1: Review previous studies on fully softened shear strength of expansive clays or similar materials
- Task 2: Sampling, geophysical surveys, and in-situ testing
- Task 3: Laboratory testing on collected samples
- Task 4: Comparison of test results and development of guidance

CHAPTER 2: LITERATURE REVIEW

2.1 Introduction

The potential for strength loss in fine-grained soils poses a significant hazard for many geotechnical projects. Damage to infrastructure attributed to strain-softening of clayey soils has been documented in many case histories involving both static (e.g., Gregersen 1981, Locat et al. 2017) and cyclic loading (e.g., Shannon and Wilson 1964, Heritage 2013, Nakamura et al. 2014). Fine-grained soils that exhibit a post-peak reduction in strength include overconsolidated clays, high plasticity clays, and marine clays that have experienced salt-water leaching (L'Heureux et. al 2014). Strength loss in high-plasticity clay soils is a common condition of the roadways in western and central Alabama and brings considerable impact including cracking of pavement and slope failures (Figure 2-1).

2.2 Landslides in High Plasticity Clays

Selecting strengths for use in slope stability analyses is often a key source of uncertainty and selected strengths must account for effects of loading conditions and any potential changes in strength over time. For slopes along highways, long-term drained strengths are often used to analyze failures that occur without significant changes in loading (Vandenberge et al. 2013, Duncan 2014), such as those observed in sites underlain by Prairie Clays. This is especially true for expansive clays, such as the Prairie clays considered in this study, where the strengths can be reduced as repeated cycles of wetting and drying occur potentially leading to failures in areas of sloping ground (Hou et al., 2013). Groundwater fluctuations have also been shown to be an

Figure 2-1: (Left) A repaired slope failure in an embankment section of SR-5 in Perry County and (right) cracking in the southbound lanes of US-231 near Laceys Spring following a large landslide in 2020.

important factor in landslide development along highways where the roadway is underlain by expansive clays (Khan and Hossain 2017, Yilmaz and Karacan 2002). Accounting for this potential strength loss when analyzing the stability of these slopes will therefore be important to obtain accurate results.

In this study, the term fully softened shear strength is defined as the peak strength of drained strength of a normally consolidated clay (Figure 2-2), which has been found to be equivalent to the long term drained strength of stiff fissured clay soils (Skempton 1970). This definition is also used by US Army Corps of Engineers (Stephens and Branch 2013). The fully softened strength is distinct from the critical state strength (Duncan 2014, VandenBerge 2013), which represents the shear strength of the soil when no further dilation or contraction occurs (Schofield and Wroth 1968). The critical state strength is usually lower than and occurs at a larger displacement than the fully softened strength (Duncan 2014), but at smaller displacements than the residual strength (Duncan 2014, Crabb and Atkinson 1991, Lupini 1981).

Several authors have examined landslide case histories to determine the appropriate strength to use in analyzing failures in clay slopes. Stark and Eid (1997) found that the fully softened shear strength was appropriate to use when analyzing first-time failures in natural cut slopes and compacted embankments. Mesri and Shahien (2003) reanalyzed a large database of slope failures in soft clays, stiff clays and clay shales to assess the mobilized shear strength. They

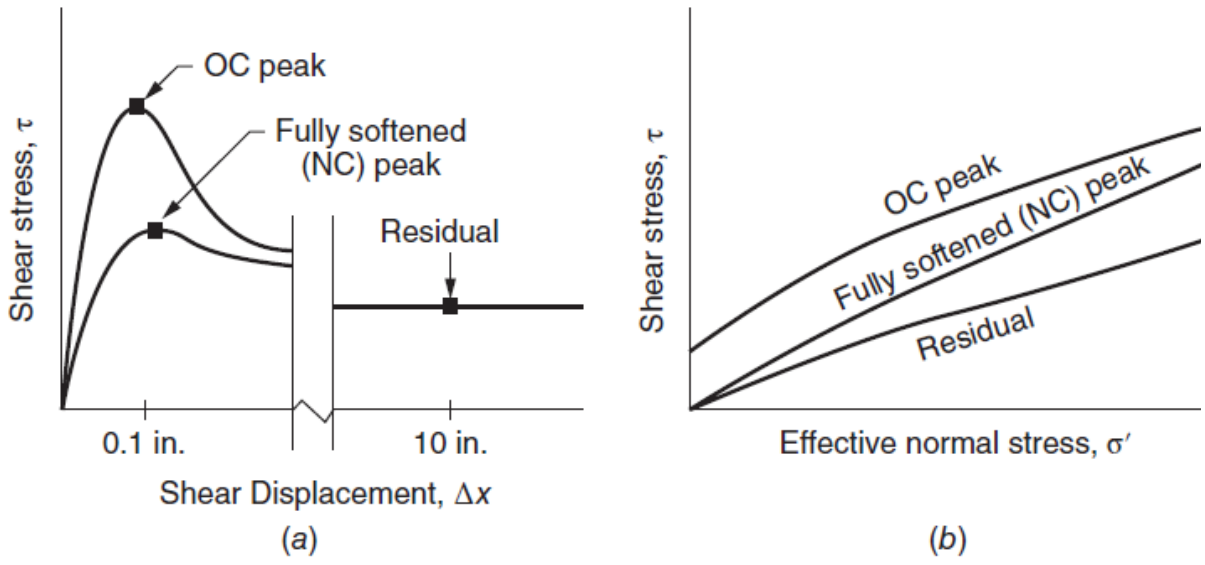

Figure 2-2: Schematic illustration of stress strain curves for softening clays showing the intact peak, fully softened, and residual strengths (Duncan et al. 2014).

found that first-time failures were primarily controlled by the fully softened strength, while residual strengths controlled reactivated landslides. Reactivated landslides are landslides that resume movement after a period of inactivity and the shearing resistance is commonly reduced to the residual condition along the entire failure surface (Mesri and Shahien 2003). Both of these studies highlighted the importance of considering the stress-dependent nature of the strength envelopes through either nonlinear envelopes or secant friction angles. A study of long-term slope stability of slopes in shale regions in the Sydney Basin found that both landslide occurrence and long-term slope stability were governed by the residual shear strengths (Dunkerley 1976). Residual strengths have also been recommended for being used for the long-term slope stability of clay soils by Skempton (1964, 1970, 1984, 1985), Tiedemann (1937) and Haefeli (1951). Correlations for both fully softened and residual shear strengths with index properties, such as the liquid limit and plasticity index, have been developed by multiple authors (Stark and Eid 1994, 1997, Mesri and Shahien 2003, Stark and Hussain 2013, Eid and Rabie 2017, Stark and Fernandez 2020).

2.3 Shear Strength Envelopes

The previous studies have highlighted the importance of measuring the drained strengths of clays to assess the long-term stability of the slopes. Drained (or effective stress) strength envelopes are commonly used to evaluate slope failures that occur due to long-term loading as opposed to loads that are applied rapidly relative to the permeability of the soil (Duncan et al. 2014). Long-term drained shear strengths of saturated soils are commonly represented in slope stability analyses using an effective stress Mohr-Coulomb failure envelope as shown in Equation 1, where the effective cohesion is typically zero for uncemented soils.

$$\tau = c' + \sigma' \cdot \tan\phi' \tag{1}$$

Where
τ = shear strength (psf or kPa)
c' = effective cohesive intercept (psf or kPa)
σ' = $\sigma - u$ = effective normal stress (psf or kPa)
σ = total stress (psf or kPa)
u = pore water pressure (psf or kPa)
ϕ' = effective angle of internal friction (deg)

Nonlinear strength envelopes can be used when a linear fit does not match the data for a particular soil. Multiple authors have highlighted the importance of considering nonlinear strength envelopes for both fully softened and residual strengths (Stark and Eid 1997, Mesri and Shahien

2003, Lade 2010) of fine-grained soils. This can be done through a stress-dependent secant friction angle or a strength envelope with a nonlinear functional form. An example of a nonlinear strength envelope is the power curve shown in Equation 2, which has been shown to work well for analyzing surficial shallow slope failures (Lade 2010).

$$\tau = a \cdot P_a \left(\frac{\sigma'}{P_a} \right)^b \tag{2}$$

Where a, b = dimensionless fitting parameters describing curvature and slope

P_a = atmospheric pressure (2116 psf or 101.3 kPa)

Correlations for the parameters a and b have been developed for fully softened strength (Stark and Fernandez 2020) and residual strengths (Stark and Idries 2021) and are available in spreadsheet form from Stark (2022).

Soils above the groundwater table will have negative pore pressures (positive suction) that will increase the effective stress and therefore the strength of the soil. This increase in strength due to suction is important for many geotechnical problems, including landslides which may be triggered by reductions in suction during rain events (Taha 2000). The total suction in soils has two primary components. The first is the matric suction, which is defined as the difference between the pore water pressure (u_w) and the pore air pressure (u_a). The second component is the osmotic suction, which is associated with the salt content of the pore water. Osmotic suction is not considered in this study as it usually has a small effect on the shear strength of soils (Leong and Abuel-Naga 2018).

The effects of suction on the strength of the soil can be included through the use of an unsaturated strength envelope (Fredlund et al. 1978) as shown in Equation 3.

$$\tau = c' + (\sigma - u_a) \cdot \tan\phi' + (u_a - u_w) \cdot \tan\phi_b \tag{3}$$

Where: ϕ_b = unsaturated shear strength angle (kPa)

u_a = pore air pressure (kPa)

u_w = pore water pressure (kPa)

At suction values below the air entry value (AEV), $\phi_b \approx \phi'$ and the unsaturated strength envelope reverts to the saturated strength envelope, but with a negative pore pressure. The AEV is defined as the matric suction value that is exceeded before air recedes into the soil pores (Fredlund and Rahardjo 1993). When matric suction exceeds the air entry value, the strength envelope for the soil can be described by Equation 3. This envelope is often assumed to be bilinear (Figure 2-3), but ϕ_b has also been shown to be dependent on the suction value resulting in a nonlinear envelope at higher suction values (Fredlund 2006). Figure 2-3 illustrates the correlation of saturated and unsaturated condition with the air entry value (AEV).

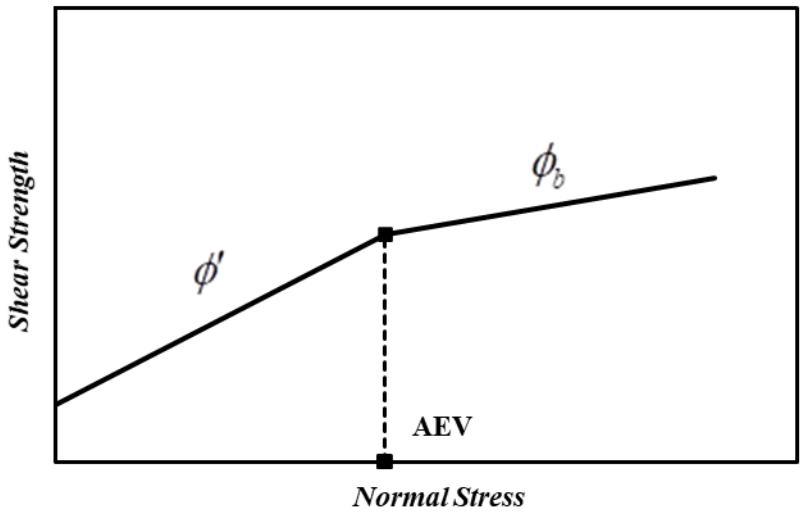

Figure 2-3: Effect of air entry value on unsaturated shear strength envelopes (Fredlund 2006).

2.4 Characterizing Landslides with Softening Clays

Detailed characterization of landslide sites is important to build models for use in slope stability analyses. An accurate assessment of site stratigraphy is needed as well as an estimation of soil properties that represent the scenario to be modeled. Site stratigraphy is typically estimated from drilling explorations that provide data only at discrete points (DeJong et al. 2016). Geophysical methods offer a means to supplement boring data and can often provide a more detailed estimation of the subsurface. Electrical resistivity imaging (ERI) provides 2D or 3D profiles of subsurface resistivity distribution which can be used to delineate clayey soils from sandy soils and rock (e.g., Loke 2004, Perrone et al. 2014). Seismic methods provide an estimate of elastic moduli via shear wave velocity measurements and are sometimes used to provide 2D or 3D profiles (e.g., Jongmans and Garambois 2007).

Standard penetration testing (SPT) can provide strength estimates for sandy soils but is not well suited for estimating properties of sensitive clays (Holtz et al. 2011). Cone penetration testing (CPT) can provide detailed information regarding soil layering and mechanical properties of soils but cannot be used at sites with significant amounts of gravel or rock intervals (Schmertmann 1978). Ring shear testing is typically used to estimate drained strength parameters of clays (e.g., Wright et al. 2007) and can provide a means for calibrating material models to expected soil behavior such as nonlinear strength, modulus reduction and damping behavior, and cyclic softening.

The data from each of these methods should be used to inform each other in a site characterization program to create geologically based models for the purpose of analysis (DeJong et al. 2016). Comparison of geophysical results to SPT or CPT provides ground truth for interpretation of soil type, site stratigraphy and geologic features identified from ERI or seismic profiles. Seismic data can also be used to guide interpretation of ERI results as soft saturated clay and fractured limestone below the water table may both exhibit low resistivity, but soft clay is expected to have a lower velocity. In-situ and lab test results can provide additional information related to soil behavior and strength in soil layers identified from the geotechnical and geophysical investigations.

2.4.1 Drilling and Standard Penetration Tests (SPT)

Drilling and sampling is primarily used to identify soil types and site stratigraphy and can provide an estimate of the water table location for landslide sites. Standard penetration testing (SPT) testing is commonly performed during drilling providing highly disturbed soil samples for classification purposes and an estimate of coarse-grained soil strength based on SPT blow counts. The SPT is performed by driving a standard split-spoon sampler a distance of 45.7 cm (18”) with a 63.5 kg (140 lbf) hammer dropped a height of 76 cm (30”) (Holtz and Kovacs 1981). The measured blow count (N) is the number of blows to drive the sampler the final 30 cm (12”). The measured blow count can then be corrected to account for overburden stress, energy ratio based on hammer type, rod length, borehole diameter and sampler liners (Bowles 1996). This process provides a corrected blow count [$(N_1)_{60}$] that allows data collected using different equipment, or at different depths, to be compared more accurately. Correlations have been developed to estimate coarse grained soil properties from SPT blow counts, but correlations can be difficult to develop for soft materials due to low blow counts and this approach cannot be used to estimate residual

strengths for clays. SPT tests are typically conducted at intervals of about 1.5m (5 ft). The SPT is therefore suitable for estimating stratigraphy, water table location and coarse-grained soil properties at landslide sites. SPT data at this site is only used to determine relative density, effective stress friction angles, and unit weights for coarse grained soil layers.

2.4.2 Cone Penetration Tests

Cone penetration testing (CPT) is a quasi-static test where a small cone is slowly (2 cm/s) pushed into the soil (Schmertmann 1978). No sample is collected, but cone tip resistance, sleeve friction, and pore pressure are commonly measured during testing (Roberston 1990). Measurements are recorded at intervals of about 5 cm (2 inches) compared to the SPT at intervals of 1.5 m (5 feet), providing nearly continuous data with depth. Correlations are available to estimate soil behavior type as well as undrained shear strength (s_u) and sensitivity (S_t) of fine-grained soils (e.g., Robertson 2009, 2016). Pore pressure measurements can also be used to estimate the water table location. The CPT is relatively fast and can provide precise estimations of soil stratigraphy, but problems can arise in very dense soils or if gravels, cobbles, or boulders are encountered (Schmertmann 1978). The CPT is therefore suitable for estimating stratigraphy, water table location and some properties of both coarse- and fine-grained layers at landslide sites.

2.4.3 Electrical Resistivity Imaging (ERI)

Electrical resistivity geophysical techniques typically utilize four electrode arrays placed on the ground surface (Figure 2-4) to provide an estimate of subsurface resistivity distribution (Loke 2004) or attached to a soil box (Figure 2-5) to estimate resistivity of materials in the lab. Known amperage is injected through two current electrodes and the resulting potential difference is measured between different pairs of potential electrodes. An ‘apparent’ resistivity distribution is then calculated using the known injected current, the potential voltage difference and a geometric factor that is related to the geometry of the selected array. This ‘apparent’ resistivity is the value of resistivity that would be measured for the given electrode geometry in a half space of homogenous resistivity. An inversion procedure is then required to estimate the true subsurface resistivity distribution from the measured ‘apparent’ resistivity values. More details on resistivity theory are outlined in Loke (2004).

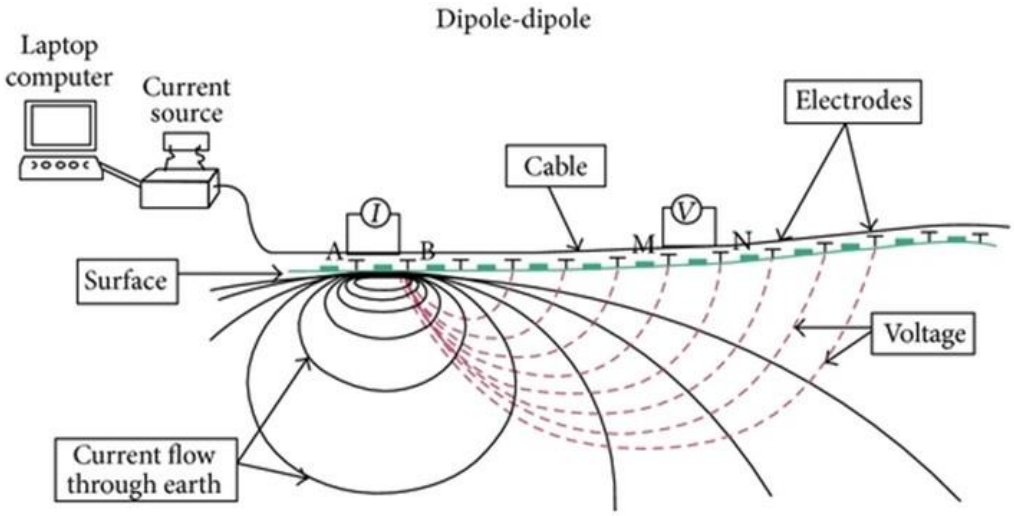

Figure 2-4: Setup for a multichannel dipole-dipole survey (Okpoli 2013).

Figure 2-5: Soil box used for resistivity testing in the laboratory.

Inversion of the field resistivity data is performed by converting the measured field data, such as potential difference (ΔV) and injected current (I), to an 'apparent' resistivity ($\rho_a = kR$) using the measured resistance ($R = \Delta V/I$) value and a geometric factor (k) that depends on the geometry of the current ($C1$ and $C2$) and potential electrodes ($P1$ and $P2$) (Loke 2004). These calculated $\rho_a$values represent the resistivity of a homogenous half space that would be measured for a given geometric factor (Loke 2004). Numerical inversion of the measured data is then required to obtain an estimate of the true subsurface resistivity distribution. The resistivity of geologic materials depends primarily on mineral content, porosity, and degree of saturation (Loke 2004).

Inversion techniques seek to find a synthetic subsurface model that produces an apparent resistivity distribution that closely matches the measured data. The starting synthetic model for

inversion of the data in this dissertation is commonly a homogenous finite element mesh with a resistivity equal to the average of the measured apparent resistivity values. The model is then updated to reduce the difference between the measured data and the model. The inversion procedure produces a non-unique estimate of the subsurface resistivity distribution as an infinite number of synthetic models may exist that fit the data equally well (DeGroot-Hedlin and Constable 1990). Resistivity data for this dissertation was inverted in EarthImager2D (AGI 2014) using a smoothness-constrained procedure known as Occam's inversion (AGI 2014). Occam's inversion seeks to find solutions that are never more complex than the true subsurface resistivity distribution (Constable et al. 1987) by producing the smoothest possible model whose apparent resistivity distribution fits the measured data to an a-priori Chi-squared statistic (AGI 2014).

The information gained from ERI surveys can be useful for characterizing landslides in several different ways. Failure planes in landslides sometimes occur near an interface between different soil strata with contrasting resistive properties which can be identified using ERI (Jongmans and Garambois 2007). Perrone et al. (2014) compiled data from 63 different landslide case histories involving ERI surveys to identify common resistive features associated with the failure masses. The failure mass is found to be less resistive than the surrounding soils in 65% of the case histories but this is primarily due to the clayey soils with high water contents involved in these failures. The failure mass is more resistive than the surrounding soils in 22% of the case and not well defined in the remaining 13% of cases. ERI has also been found useful for identifying critical layers in landslides involving marine clays. Marine clays can attain high degrees of sensitivity due to saltwater leaching. Leaching of the saltwater makes the clay less conductive allowing the most sensitive zones in a marine clay slope to be identified as having relatively higher resistivity values than surrounding clays in an ERI profile (L'Heureux et. al 2014). Disadvantages associated with ERI include loss of resolution with depth, results that are not easily correlated to geotechnical properties, and an inversion process is required which produces a non-unique solution (Jongmans and Garambois 2007).

2.4.4 Multi-Channel Analysis of Surface Waves (MASW)

Multi-channel analysis of surface waves (MASW) is a seismic-based geophysical method, which takes advantage of the velocity and frequency characteristics of surface waves. A benefit of seismic methods is they provide a direct estimate of shear wave velocity (Uhlemann et al. 2016). MASW surveys typically utilize 24 or 48 evenly spaced geophones to record ground velocity (Park

et al. 1999). Active surveys can be performed using an input source, such as sledgehammer on a plate (Figure 2-6) and have investigation depths of about 10 m to 40 m depending on site conditions (Park et al. 1999). Passive surveys do not use an active source but instead measure vibrational noise from the environment such as traffic vibrations along a highway and can measure much deeper than active surveys (Park and Miller 2008). More details regarding MASW data collection can be found in Park et al. (1999).

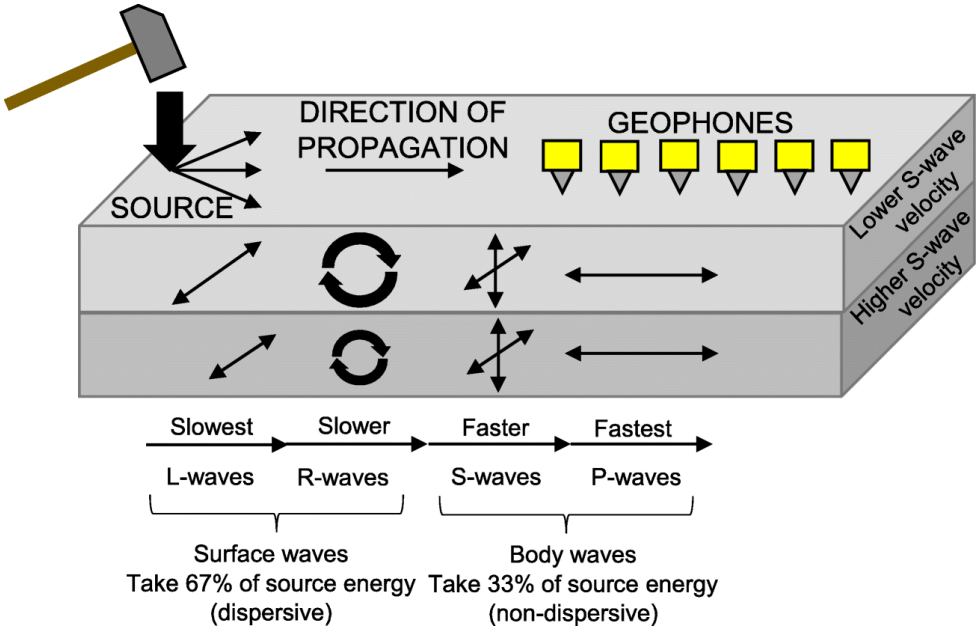

Figure 2-6: Body and surface seismic waves generated by a sledge hammer (seismic source) and received by an array of geophones (receivers). Simplified directions of particle motion in the ground are shown for a two-layer system (Jug et al. 2020).

Shear wave velocities are estimated from MASW results through an inversion process (Reynolds 2011). A vital step when processing MASW data is to determine a dispersion curve which relates wave energy to frequency content and phase velocity (Park et al. 2011). Dispersion images are often generated using commercial software, but the user is still required to select an appropriate dispersion curve which can be difficult. Several modes may exist in a dispersion image (Gao et al. 2015) but proper selection of the fundamental mode is important for an accurate estimation of shear wave velocity (Wathelet 2005). Once the dispersion curve is selected it is used in an inversion procedure to obtain a shear wave velocity profile. The inversion procedure requires estimations of an initial earth model, soil density and Poisson's ratio (Park et al. 1999). Further details regarding inversion of MASW data can be found in Wathelet (2005).

Resolution of the MASW profiles near the surface depends on the shortest wavelengths (highest frequencies) that can be represented in the dispersion curve which is controlled by the geophone spacing (Lin et al. 2004). The shortest wavelength required to detect a surface layer of a given thickness is equal to twice the minimum surface layer thickness and the geophone spacing required to estimate shear wave velocity is equal to the surface layer thickness (Park et al. 1999). This means that a geophone spacing of 1 m is required to detect surface layers as small as 1 m thick and to represent wavelengths as small as 2 m. The shortest wavelength represented in the dispersion curve may also be estimated from the highest frequency on the selected dispersion curve and the corresponding velocity. Soil layers thinner than the geophone spacing may be detected at greater depths due to the interaction of surface waves with differing frequencies and velocities. The maximum depth of investigation for a MASW survey depends on the longest wavelength (lowest frequencies) measured by the geophones which depends on the frequency characteristics of the subsurface and the seismic source and the survey length (Taipodia et al. 2018).

Seismic methods are often used in conjunction with ERI to investigate landslides. Jongmans and Garambois (2007) compiled data from geophysical landslide investigations and show that the seismic velocities of the failure mass tend to be lower than the surrounding soils, allowing the geometry of the failure mass to be estimated using seismic methods. Disadvantages of seismic methods include complex processing, which is time consuming and subject to user interpretation. Data collected along roadways may also be affected by vibrational traffic noise (Kiernan et al. 2021). For surveys along highways, the effects of traffic noise can be reduced by timing shots to occur during relatively quiet periods between large vehicles. As with ERI, the inversion process for seismic data is uncertain and the inverted solution is non-unique.

2.5 Analysis of Landslides Involving Softening Clays

Slope stability analyses are typically performed using Limit Equilibrium Methods (LEM) or Strength Reduction Methods (SRM) for cases involving static loading of slopes. LEM typically uses the method of slices to solve for a factor of safety (FS) and a search algorithm to find the critical failure surface. Assumptions regarding the location and shape of the slip surface as well as the interaction of interslice forces are required for LEM. SRM does not require a search algorithm to find the critical failure surface and slices are not utilized so assumptions regarding interslice forces are not needed. The critical failure surface in SRM is determined through calculation of element stresses in the numerical model. The use of nonlinear deformation analyses (NDAs) is

needed if estimates of displacements are required. The full equations of motion are solved in NDAs in order to estimate deformation patterns and magnitudes. Advanced constitutive models may also be utilized in NDAs to represent element level soil behavior that is important to the problem being analyzed. NDAs are more commonly used for earthquake-induced landslides (e.g., Kiernan 2021) and are not considered in this study.

2.5.1 Limit Equilibrium Method (LEM)

LEM analyses may be used to determine the FS of a slope. Traditional LEM typically utilize a method of slices which divide the slope into a number of vertical slices (Duncan et al. 2014). The vertical slices are then used to compare driving stresses to shear resistance at different points on a given failure plane which are used to determine equilibrium of the slope. An iterative procedure is then implemented which analyzes various possible slip surfaces to determine a critical failure surface, which is commonly the surface with the minimum value of FS (Duncan 1996).

Various procedures are available for performing the method of slices calculations and each makes assumptions regarding the shape of the failure surface and interslice forces acting between each slice. A few of these methods are discussed below but many more are procedures exist and are readily available for use in common slope stability programs (e.g., Rocscience 2021). The Ordinary Method of Slices assumes a circular failure surface, neglects interslice forces, and satisfies only moment equilibrium about the center of the circle (Duncan et al. 2014). The simplified Bishop's method assumes a circular failure surface, assumes interslice forces act horizontally, and satisfies moment equilibrium about the center of the circle as a well as vertical force equilibrium for each slice (Duncan et al. 2014). Spencer's method can account for slip surfaces of any shape and assumes forces between each slice act parallel to each other at some unknown inclination (Duncan 1996). The inclination of the interslice forces is determined through solution of equilibrium equations (Spencer 1967). Spencer's method satisfies equilibrium of moments as well as equilibrium of forces in the horizontal and vertical directions (Spencer 1967).

2.5.2 Strength Reduction Method (SRM)

The strength reduction method (SRM) may be used to determine the FS of a slope (Itasca 2016). The SRM is a form of limit equilibrium analysis that is typically implemented within a finite element (FEM) or finite difference (FDM) program (Duncan et al. 2014). To perform the calculation, multiple analyses of a single slope are performed using different strength values in order to find the boundary between equilibrium and instability. This boundary is often defined

using a velocity or displacement threshold or if the numerical solution fails to converge (Duncan et al. 2014). The FS of the slope may then be defined as the ratio of the actual shear resistance of the soil to the shear resistance required to produce the unstable condition (Dawson et al. 1999). SRM has several advantages over traditional limit equilibrium based on the methods of slices. No slices are utilized so assumptions regarding interslice forces are not required (Duncan et al. 2014). SRM also does not require any assumptions or search algorithm for the critical failure surface as the location of the failure plane in FEM and FDM analyses is determined through calculation of element stresses in the numerical model (Griffiths and Lane 1999). Slope displacements and velocities can be plotted using SRM, but these values should be used to assess instability and identify failure surfaces and not to estimate actual deformation magnitudes or rates.

2.5.3 Nonlinear Deformation Analysis (NDA)

NDAs typically utilize FEM or FDM that differ from the methods discussed above in that they solve the full equations of motion to estimate deformation patterns and magnitudes (e.g., Beaty and Dickenson 2015, Boulanger and Montgomery 2016, Mohammadi and Taiebat 2016, Zabolotnii et al. 2021). NDAs require a numerical solver (e.g., FEM or FDM) and a constitutive model to represent the material behavior. NDAs can also handle dynamic loading (e.g., Beaty and Dickenson 2015, Montgomery 2015) as well as interaction between the soil and reinforcing elements (e.g., Yu et al. 2015, Chaudhary et al. 2016), deep foundations (e.g., Chen and Martin 2002, Ghorbani et al. 2019) or surface structures (e.g., Reza Tabatabaiefar et al. 2013, Pinzón et al. 2020). There use in practice for static slope stability problems is still rather limited due to the time and effort required to build a simulation and limitations in analyzing large deformation problems.

CHAPTER 3: CHARACTERIZATION OF COLLECTED SAMPLES

3.1 Introduction

The literature review has highlighted the need to examine both fully softened and residual strengths for evaluating landslides in high plasticity clays. This chapter focuses on the laboratory and geophysical testing of samples collected from the selected sites. Several different tests were performed on the samples to characterize the index properties, mineralogy, and electrical resistivity. This chapter first describes the collected samples, followed by a discussion of the test methods and a summary of the obtained results. Further details on the testing methods will be published by Xuan (2023).

3.2 Selected Sites

Samples for laboratory testing were collected from six sites (Figure 1-1) where landslides had either been observed or pavement cracking had been observed and previous studies had suggested a landslide may be occurring (Kennedy 2019). Electrical resistivity measurements were performed at five of the sites and MASW tests were performed at three. Borings were performed at each of the sites to collect samples and the boring numbers and approximate coordinates of the site are listed in Table 3-1.

Table 3-1: Locations selected for laboratory testing

Route	Milepost	Approximate Coordinates	Observations	Boring	Geophysical Surveys
SR-5	53.1	32.51185, -87.37282	Pavement Cracking	B-5.5A	ERI
SR-22	62.0	32.83092, -86.71142	Landslide	B-3	
SR-219	35.9	32.87873, -87.10227	Landslide	B-2, B-3	ERI, MASW
I-59	80.4	33.17520, -87.40238	Landslide	B-1	
US-231	35.9	34.53320, -86.58983	Landslide	SB4-1	ERI, MASW
I-65	87.4	31.35989, -87.06662	Landslide	B-6, B-7	ERI, MASW

3.3 Index Testing

Each of the collected samples was tested to determine both the Atterberg Limits and clay fraction. These tests followed the procedures outlined in ASTM D4318 (2018) for liquid limit and plastic limit and ASTM D7928 (2017) for hydrometer. The results from these tests are shown in Table 3-2.

Table 3-2: Index test results for the collected samples

Site	Boring	Depth Range (ft)	Liquid Limit (LL)	Plasticity Index (PI)	Clay Fraction (%)	Activity
SR-5	B-5.5A	1-7	86	60	58.5%	1.02
SR-22	B-3	12-13.5	48	21	40.9%	0.51
SR-22	B-3	9-10.5	51	26	35.6%	0.73
SR-219	B-2	38.5-39.9	46	23	41.2%	0.56
SR-219	B-3	19-20.5	50	24	53.5%	0.45
I-59	B-1	33.5-35	65	30	67.8%	0.44
US-231	SB4-1	35.5-36	45	20	40.9%	0.49
US-231	SB4-1	36.4-37	46	18	40.7%	0.44
I-65	B-6	4.5-6	116	63	86.7%	0.73
I-65	B-7	4.5-6	102	60	83.8%	0.72
I-65	B-7	7.5-9	115	59	94.4%	0.62
I-65	B-7	13.5-15	105	55	83.6%	0.66

3.3.1 Atterberg Limits

The Atterberg Limits for each of the samples is shown in Figure 3-1 along with the USCS classifications and common ranges of clay minerals (after Holtz et al. 2011). Samples from sites on SR-5, I-59, and I-65 classify as high plasticity clay or silt (liquid limit greater than 50), while the samples from US-231, SR-22, and SR-219 classify primarily as low plasticity clays.

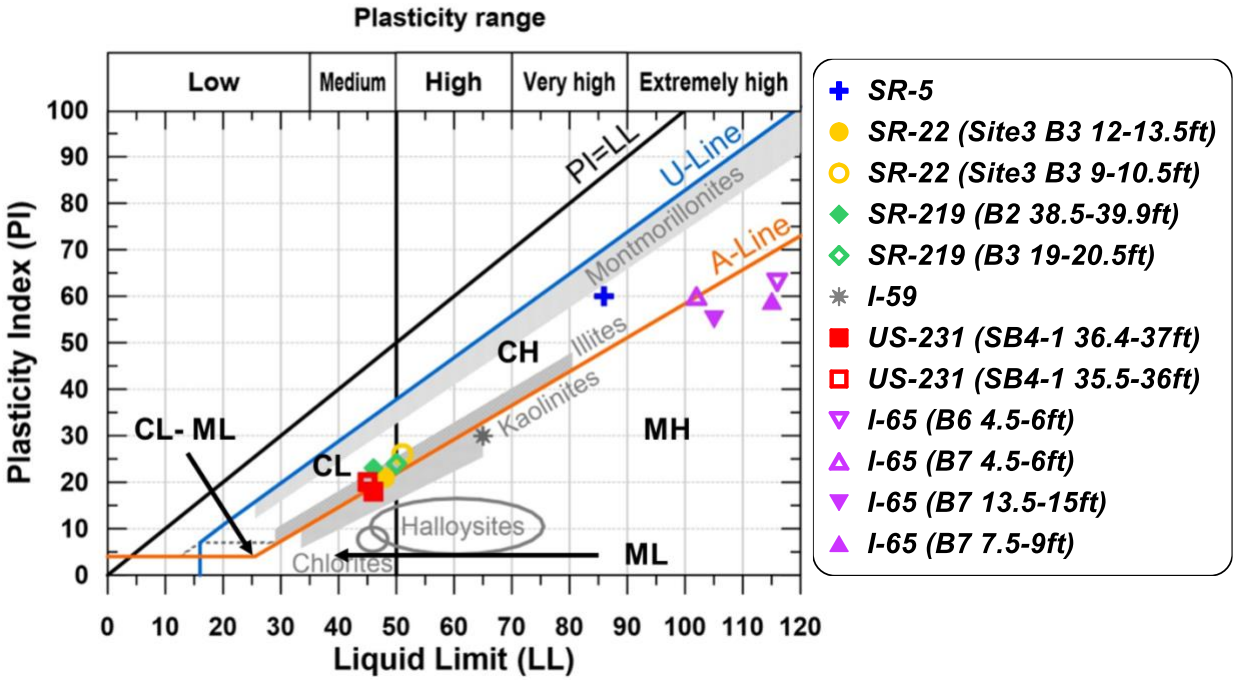

Figure 3-1: Atterberg Limit results for the collected samples along with boundaries for different classifications and common ranges for different minerals (after Holtz et al. 2011).

3.3.2 Clay Fraction and Activity

The clay fraction and activity (PI / Clay Fraction) of the samples is also shown in Table 3-2. Activity can be useful for assessing how important the influence of the clay fraction is on the overall properties of the clay and can be correlated with engineering behavior (e.g., swelling potential) and mineralogy (Mitchell and Soga 2005). The activities for the sites considered in this study fall into three main categories. SR-5 has the highest activity and falls on the lower end of range normally seen for smectite clays, such as montmorillonite (Mitchell and Soga 2005). Samples from I-65 and the shallower sample from SR-22 all show activities between 0.6 and 0.75, which would be more typical of illite clays (Mitchell and Soga 2005). This range would also be typical for attapulgite and allophane clays, but these are not expected to occur in the study area. The other samples (US-231, I-59, SR-219, and the lower depth from SR-22) have activities ranging from 0.44 to 0.56, which would be more typical of kaolinite clays (Mitchell and Soga 2005) or mixtures of kaolinite and illite. These correlated mineralogy results are consistent with the approximate ranges for the various clay minerals shown in Figure 3-1.

3.4 XRD Testing

The index testing provided some information about the potential mineralogy of the samples, but a more quantitative analysis of mineralogy was achieved using X-ray diffraction (XRD) testing. X-ray diffraction is an important tool used to characterize crystalline substances (e.g., minerals). Crystalline substances consist of parallel layers of atoms and radiation entering the substance will be scattered (diffracted) by these layers. By measuring the diffraction pattern at different incident angles between the beam and the mineral surface, information on the crystal structure and the spacing between the crystalline sheets can be obtained. This process can be very useful for identifying clay minerals and a summary of using XRD for this purpose is provided by Mitchell and Soga (2005).

The XRD testing performed for this study was conducted using equipment in the Geosciences department at Auburn University and generally followed the procedures described by Poppe et al. (2001) for clay mineral identification. Clay samples were prepared by ball milling the dried clay to form a powder and then mixing the powder with distilled water. Samples were then placed in a centrifuge to settle the clay minerals. The clay solution was spread onto glass slides and air dried for 24 hours. The preparation of the slides after this depended on the test. Some slides were treated with ethylene glycol to expand swelling clays, while others were heated to either 400°C or 550 °C. This heating can reveal changes in the spacings of the crystal structure due to

dehydration of the clay minerals. Different minerals will react differently to the various preparations (e.g., Figure 3-2) and Poppe et al. (2001) provide flowcharts for identifying dominant clay minerals based on these changes. After preparing the slides, the samples were placed in a Bruker D2 PHASER benchtop diffractometer for analysis.

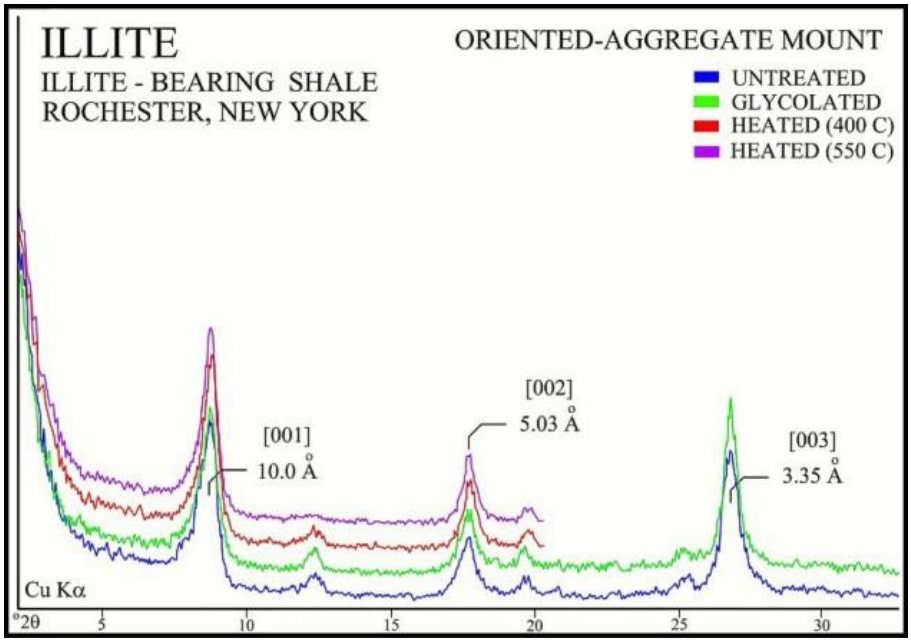

Figure 3-2: XRD results of illite clay subjected to different treatment methods prior to testing (Poppe et al. 2001).

XRD testing was performed on five of the samples (Figure 3-3 - Figure 3-7) to confirm the correlated mineralogical results based on the Atterberg Limits and activity discussed in the previous section. The mineralogical results from the XRD testing are summarized in Table 3-3. The XRD results largely agree with the correlations based on activity, especially when considering that many of the samples showed more than one constituent. Montmorillonite-illite is one of the most common mixed-layer clays (Mitchell and Soga 2005) and is seen in the XRD results at both I-65 and SR-22. The Atterberg Limits of these two sites are very different with the samples from I-65 showing much higher LLs, likely indicating these samples have a larger proportion of montmorillonite. The samples from US-231 standout as the XRD indicates the presence of chlorite, while the Atterberg Limits (Figure 3-1) do not. The results for US-231 are discussed in more detail below.

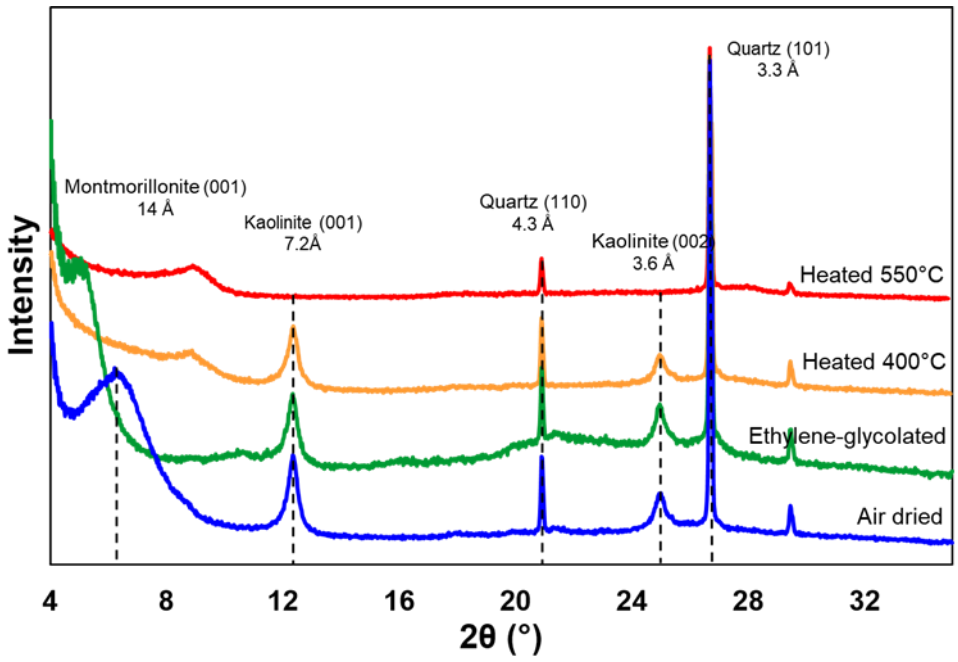

Figure 3-3: XRD results for sample collected from SR-5 (B-5.5A, 1-7 feet).

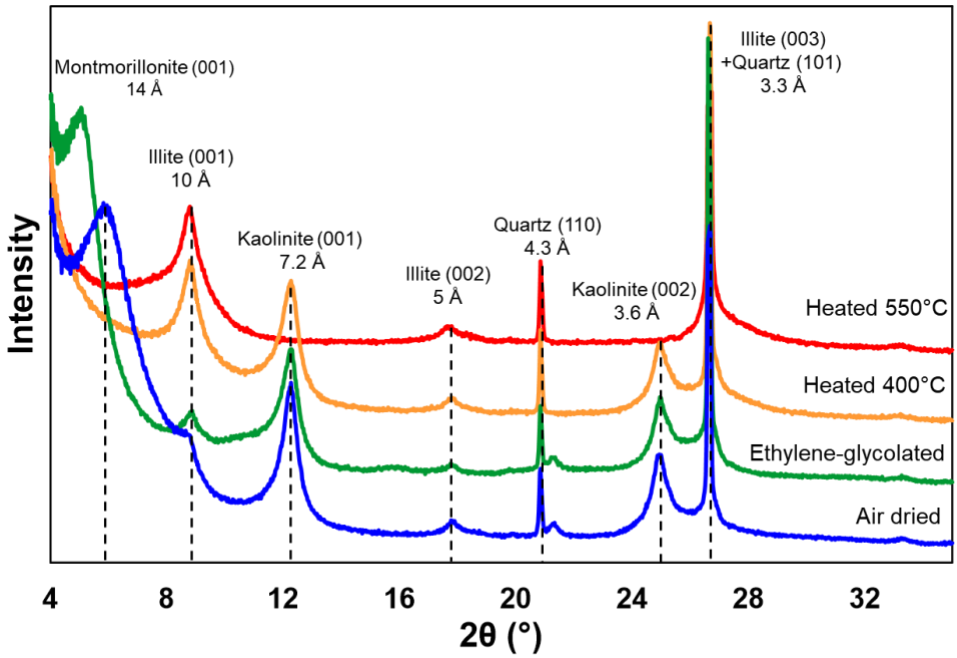

Figure 3-4: XRD results for sample collected from SR-22 (B-3, 9-10.5 feet).

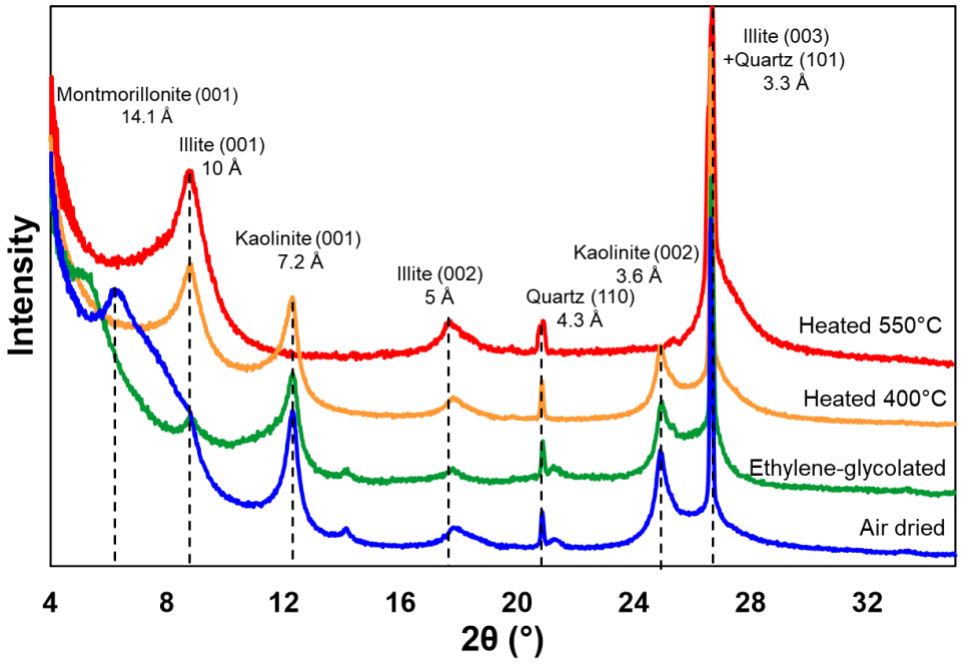

Figure 3-5: XRD results for sample collected from I-59 (B-1, 33.5-35 feet).

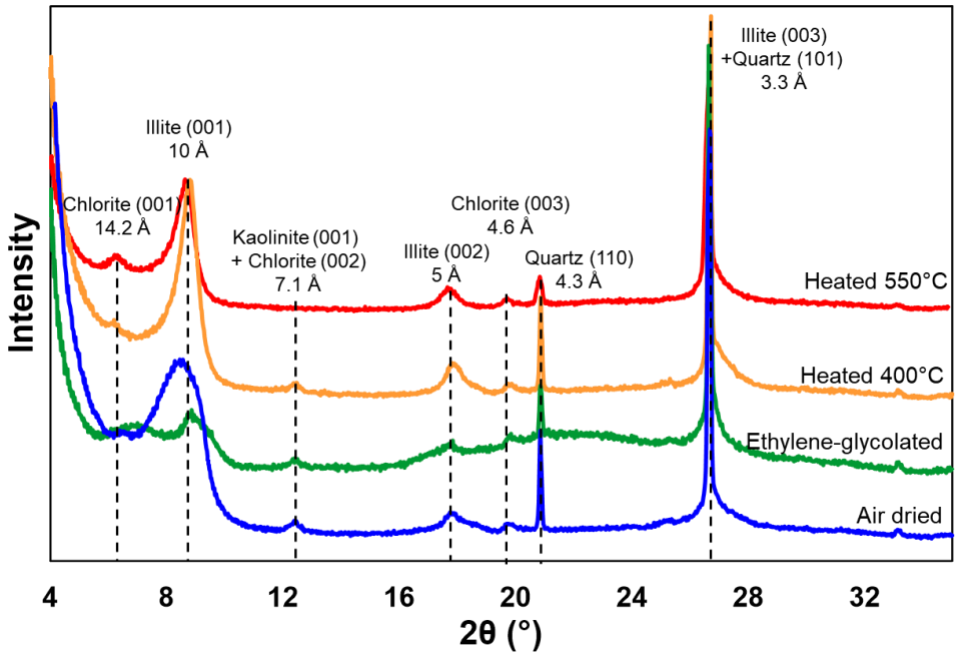

Figure 3-6: XRD results for sample collected from US-231 (SB4-1, 35.5-36 feet).

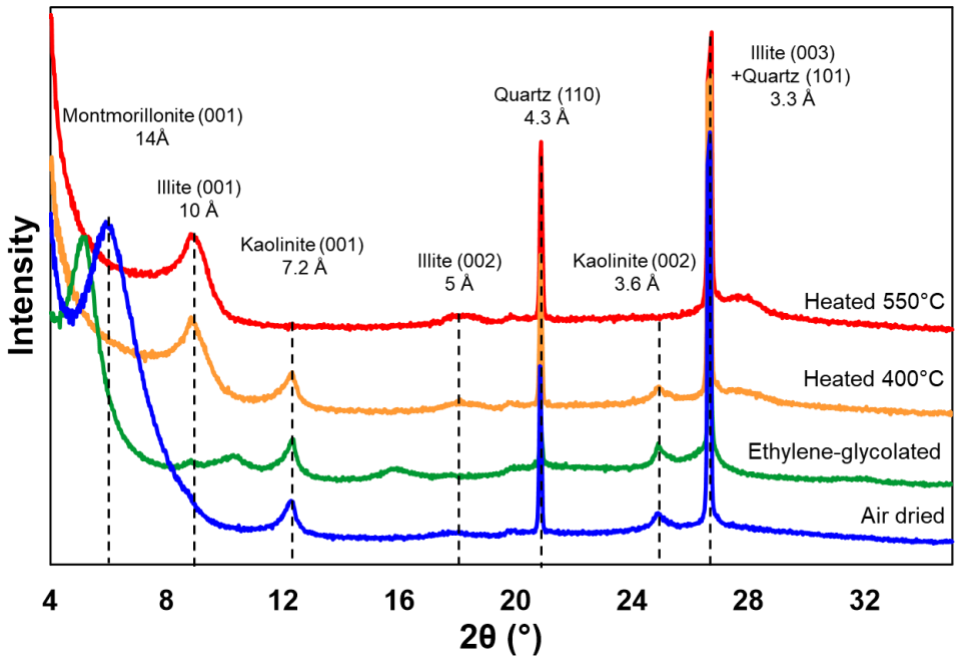

Figure 3-7: XRD results for sample collected from I-65 (B-7, 4.5-6ft).

Table 3-3: Clay mineralogy results

Site	Boring (Depth)	Depth Range (ft)	Correlations Based on Activity	XRD Results		
				Mineral 1	Mineral 2	Mineral 3
SR-5	B-5.5A	1-7	Montmorillonite	Montmorillonite	Kaolinite	Chlorite
SR-22	B-3	12-13.5	Kaolinite or Illite	Not tested		
SR-22	B-3	9-10.5	Illite	Montmorillonite	Illite-montmorillonite or illite-vermiculite	Kaolinite
SR-219	B-2	38.5-39.9	Kaolinite or illite	Not tested		
SR-219	B-3	19-20.5	Kaolinite or illite	Not tested		
I-59	B-1	33.5-35	Kaolinite or illite	Illite-vermiculite	Kaolinite	Chlorite
US-231	SB4-1	35.5-36	Kaolinite or illite	Illite-montmorillonite or illite-vermiculite	Chlorite	Kaolinite
US-231	SB4-1	36.4-37	Kaolinite or illite	Not tested		
I-65	B-6	4.5-6	Illite	Not tested		
I-65	B-7	4.5-6	Illite	Montmorillonite	Illite-montmorillonite or illite-vermiculite	Kaolinite
I-65	B-7	7.5-9	Illite	Not tested		
I-65	B-7	13.5-15	Illite	Not tested		

The XRD results for US-231 were interesting as this was the only sample that showed a significant amount of chlorite. The samples of soil from US-231 were taken from a weathered shale or mudstone layer that was consistent with the depth of the sliding plane. This zone is within the Pennington formation, which is a Mississippian age formation and consists of primarily shale with interbedded limestone, dolomite, sandstone, mudstone, and minor coal (Szabo et al. 1988). The upper sample used in this study had a purple color, while the lower sample was grey. Both samples had similar Atterberg Limits and similar strengths as discussed later. The Atterberg Limits and activity fall within the ranges usually associated with kaolinite or illite, while the XRD for the purple sample shows primarily mixed illite layers and chlorite. Illite and chlorite have similar structures, but chlorite has an extra octahedral sheet making it a 2:1:1 clay mineral (Mitchell and Soga 2005). This extra octahedral sheet reduces the cation exchange capacity relative to illite and vermiculite and the liquid limit of chlorite is lower than illite. The plasticity index of chlorite is also usually low with some samples being non-plastic. The LL for the US-231 samples is within the range expected for chlorite, but the PI is quite a bit higher (Table 3-4) and more consistent with that expected for illite.

Table 3-4: Clay mineralogy results

Soil/Mineral Type	**Liquid Limit (LL)**	**Plasticity Limit (PL)**	**Source**
US-231 (SB-4, 35.5-36)	45	20	This study
Illite	60 - 120	35 - 60	Mitchell and Soga (2005)
Chlorite	44 - 47	36 - 40	Mitchell and Soga (2005)
Vinton County, OH	47 - 62	23 - 33	Webb and Collins (1967)
Lewis County, WV	38 - 54	29 - 39	Okagbue (1986)

The Atterberg Limits and XRD results for the US-231 sample are consistent with similar soil found at landslide sites in Ohio (Webb and Collins 1967, Fisher et al. 1968, Wu et al. 1993) and West Virginia (Okagbue 1986). All three of these studies investigated landslides occurring within shale and/or mudstone layers within Mississippian or Pennsylvanian age formations. Illite and chlorite were also found to be the main mineral constituents, but the illite was found to be degraded due to the loss of potassium and abundance of ferric iron. Pomeroy and Thomas (1985) performed XRD testing on samples collected from the Pennington Formation in northern Alabama and determined that this deposit also contained degraded illite, which were likely to be unstable.

3.5 Electrical Resistivity

The electrical resistivity of selected samples was measured in both the field and the laboratory. Previous studies have demonstrated that the electrical resistivity of a clay can be correlated with its cation exchange capacity and therefore the mineralogy of the sample (e.g., Russell and Barker 2010, Gunn et al. 2015, Kibria and Hossain 2019). For the current study, resistivity was measured using an AGI SuperSting R8. In the field, surveys were performed using 56 electrodes and dipole-dipole and/or strong gradient arrays. Details on the equipment and common field practices for these resistivity tests are provided by Montgomery et al. (2020).

Laboratory resistivity measurements were performed using a soil box (Figure 3-8) and a Wenner four-electrode measurement (ASTM G57 2020). The SuperSting measured the resistance of the soil, which was corrected for temperature effects using Equation 3-1 and converted to resistivity using the geometric factor of the soil box.

$$R_{15.5} = R_T\left(\frac{25+T}{40}\right) \quad (3\text{-}1)$$

$R_{15.5}$ - Resistance of the soil at a temperature of 15.5°C (Ω)
R_T – Measured resistance (Ω)
T – Temperature in °C

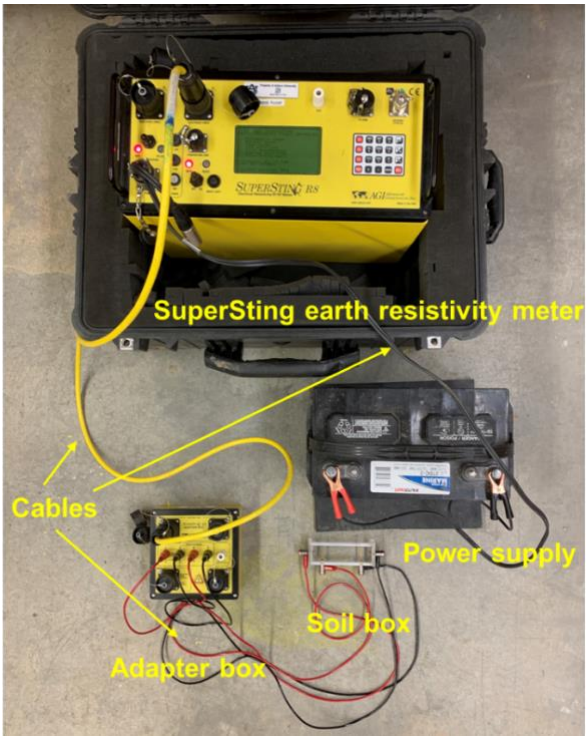

Figure 3-8: Equipment for measuring electrical resistivity of soil samples in the lab.

Samples were prepared at different water contents by mixing the clay with different amounts of deaired water. This ensured that the chemistry of the pore water was the same for all of the samples. Different water contents were considered as previous studies have shown that the resistivity of soil tends to increase as soils become drier (e.g., Kibria and Hossain 2019). The results for the tested soils are shown in Figure 3-9. Each of the soils reaches a minimum resistivity over a range of intermediate water contents. The resistivity of the samples resistivity sharply increased below this range of water contents due to the soil becoming dryer and increasing slightly increase at water contents above this range due a decrease in the density at high water contents. The minimum resistivity generally occurred at a water content between the LL and PL.

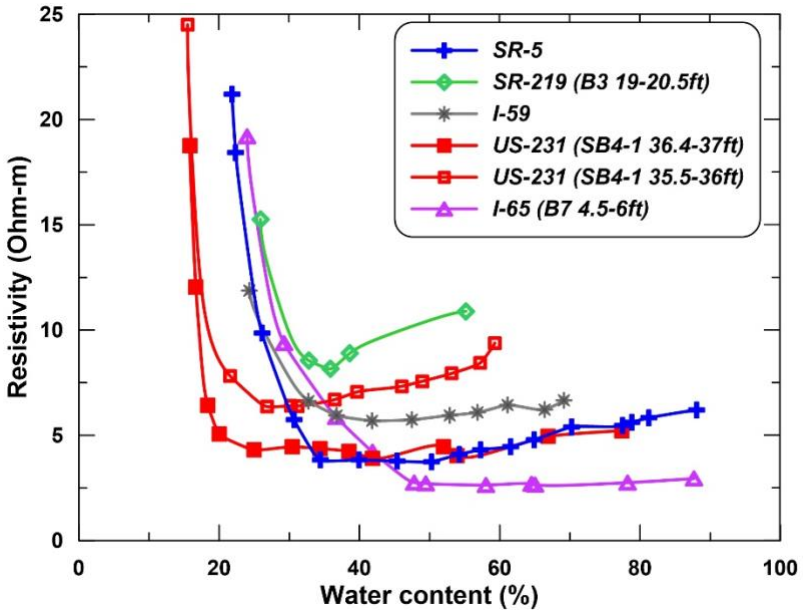

Figure 3-9: Resistivity results for selected samples as measured in the lab at different water contents.

The minimum resistivity results in Figure 3-9 fall into three main categories. The resistivity of samples from I-65, US-231 (36.4 – 37 feet), and SR-5 were all less than 5 ohm-m over a large range of water contents. Samples from US-231 (35.5 – 36 feet) and I-59 were near 5 ohm-m and the sample from SR-219 was near 8 ohm-m. Field surveys at these sites showed consistent results with the laboratory measurements as shown in Figure 3-10 through Figure 3-13. The lower end of this range is consistent with the resistivity of bentonite (montmorillonite) which is 2 - 3 ohm-m (Russell and Barker 2010, Kibria and Hossain 2019). Illite has a resistivity close to 8 ohm-m, while kaolinite ranges from 30 – 90 ohm-m (Kibria and Hossain 2019, Russell and Barker 2010).

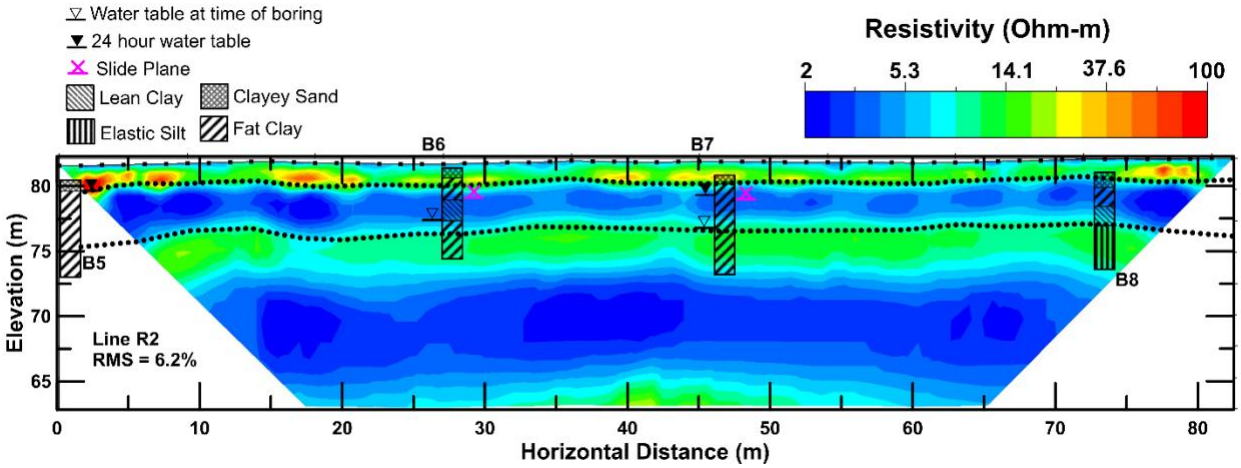

Figure 3-10: Results from survey R2 at I-65. The lowest resistivity value within the upper clay layer is 2 ohm-m.

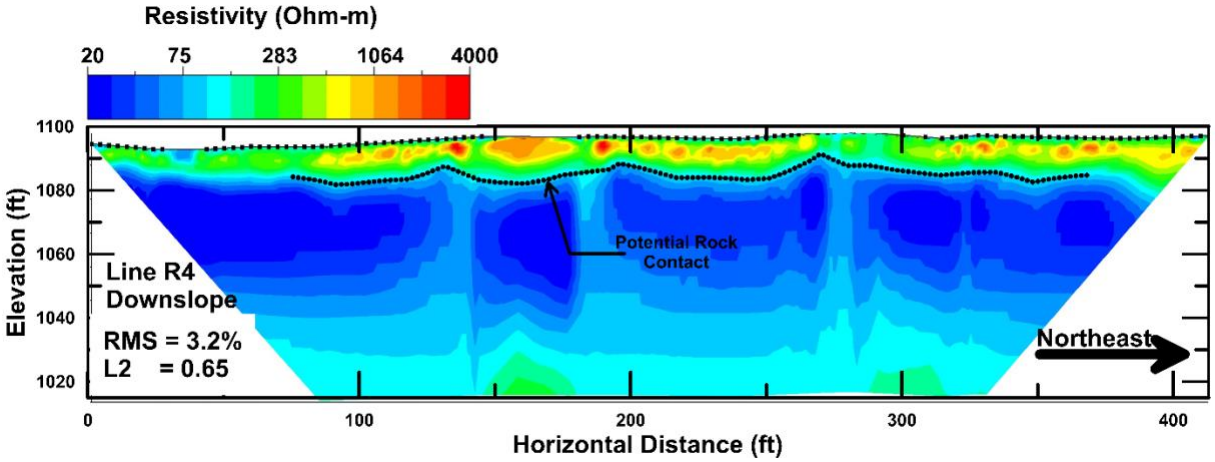

Figure 3-11: Results from survey R4 at US-231. The lowest resistivity value within the weathered rock is 8 ohm-m.

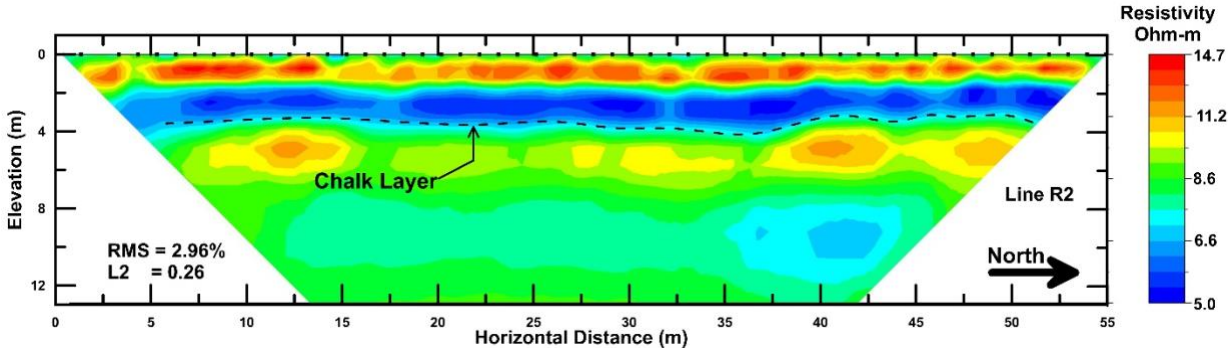

Figure 3-12: Results from survey R1 at SR-5. The lowest resistivity value within the clay layer is 5 ohm-m.

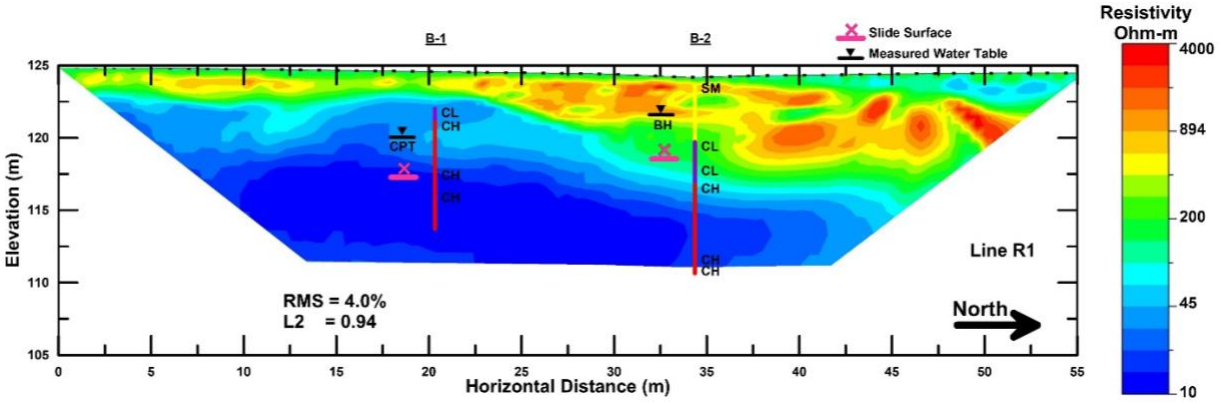

Figure 3-13: Results from survey R1 at SR-219. The lowest resistivity value within the clay layer is 7 ohm-m.

3.6 Shear Wave Velocity

MASW testing was performed at three of the sites (I-65, US-231, and SR-219) and to measure shear wave velocities of the soil in-situ. At I-65, the velocity within the clay layer varied from 200 ft/s – 425 ft/s. The lower end of the range is believed to be the location of the slide plane. For US-231, the clay layer was located approximately 30 – 40 feet below the roadway, which limited the resolution. At this depth range, the velocity varied from 750 ft/s – 1230 ft/s. At SR-219, the clay layer had velocities ranging from 640 ft/s to 800 ft/s. It is difficult to compare these velocities as they were measured at different depths and different field conditions. It is clear that the velocity at I-65 is significantly lower than the other two, which is consistent with the soft weak clay at this location.

3.7 Summary

Samples of clay collected at sites in west and north Alabama were characterized using index tests, geophysical measurements, and XRD. The results showed that the most common clay mineral is illite, with samples from I-65 in Conecuh County and SR-5 in Perry County showing larger proportions of montmorillonite. Clay samples from US-231 near Laceys Spring were unique in that the Atterberg Limits were similar to results collected at SR-219 in Bibb County, but the resistivity results were close to a sample from I-59 in Tuscaloosa County, which had a much higher LL and PI. XRD results showed that sample from US-231 is likely a degraded illite, which has been found in similar geologic units in eastern Ohio, western Pennsylvania and West Virginia. Degraded illites can classify as a low activity clay but have similar properties to montmorillonites (Fisher et al. 1968). The strength properties of these samples will be described in the next chapter.

CHAPTER 4: RING SHEAR TESTING

4.1 Introduction

One of the key tasks in the current project was ring shear testing to measure fully softened and residual drained strength envelopes for the clays. This test is performed by placing a remolded soil specimen in a steel ring between two porous stones (Figure 4-1). The upper stone is then rotated relative to the bottom stone to shear the specimen. The specimen and porous stone interface are important as the porous stone should not slide across the surface of the soil (Stark 2017). For the current study, brass porous elements were machined to have a rough surface (Figure 4-1b), as recommended by Stark (2017), to ensure that the torsional loading was properly transferred to the soil specimen. Details on the machining of the porous stones are discussed by Kennedy (2019). Normal stress is applied using a counter balanced lever loading system. The shear loading is applied at a slow rate to assure drainage of any excess pore pressures. The tests for this study were performed in general accordance with the procedures discussed in ASTM D6467 (2013) using the "flush" procedure, which ensures the top porous stone remains approximately flush with the surface of the specimen container. All tests were performed on saturated specimens. Details on the testing procedure used for this study are discussed in the next section. Only one test is performed for each specimen as recommended by previous researchers (Stark and Vettel 1992).

(**a**) (**b**)

Figure 4-1: Torsional ring shear apparatus (**a**) Controls Group Bromhead ring shear apparatus; (**b**) modified porous stones used in this study.

4.2 Sample Preparation and Testing Procedure

To prepare the soils for ring shear testing, the samples were first oven dried and sieved through a No. 40 sieve to remove any large particles to ensure the uniformity. Deaired water was added to the material until a target average gravimetric water content was achieved which corresponded to a saturated condition and a liquidity index (LI) of approximately 0.6 to minimize trapped air during placement of soil into the container. A higher gravimetric water content could not be achieved as the soils were too soft to then prepare a specimen for testing. Once the soil was prepared with the correct water content, the material rehydrated for at least 24 hours in a humidity-controlled environment. The masses of the empty specimen container, porous stones, and top platen were recorded prior to each test. After rehydrating for 24 hours, the soil was placed into the specimen container using a spatula and a razor blade was used to cut the soil flush with the top of the specimen container. The specimen and container were weighed to determine the amount of soil in the container. The specimen and container were then placed in the ring shear device and the water bath was filled to submerge the specimen in order to prevent specimen from drying and to maintain saturation during testing. Preconsolidation loads were placed on the loading arm and the vertical displacement was monitored. The magnitude of the preconsolidation load was based on the available weights with the requirement that it be less than the consolidation load used for the shearing phase. The load was left in place for ten minutes or until vertical movements had stopped.

Tests were performed at various stress levels in order to characterize the strength envelopes across a wide range of effective stresses. The specific stress values used in the testing program were based on the available loading weights. The specimen consolidated for 24 hours under the applied load or until the consolidation process was complete as judged from the settlement rate. According to ASTM D6467 (2013), specimens must not settle more than 15% of the initial specimen height during consolidation. For the device used in this work, this would correspond to a maximum settlement of 1.2 mm. The maximum settlement for this study was set as 0.75 mm to be conservative relative to the standard and tests with settlements larger than this were not used. When consolidation was complete, shear was applied using a rotational rate that was appropriate for the soil being tested (ASTM D6467 2013). Data was recorded for 24 hours or until a well-defined residual strength state was obtained. After shearing, the top platen was carefully separated from the specimen to check that a well-defined failure plane had formed. Tests without a well-defined failure plane within the soil were discarded. Both the fully softened (peak shear stress) and

residual (average shear stress after reaching residual state) shear stresses were recorded from each test. Additional details on the testing process are discussed by Xuan (2023).

4.3 Ring Shear Testing Results

The test results are shown in Figure 4-2. The remolded samples quickly reach a peak followed by a large drop in strength. This peak is defined as the fully softened strength of the soil. After a certain amount of shear displacement (approximately 0.5 – 2.0 inches for the tests in this study), the shear stress is approximately constant, and the sample is assumed to have reached a residual strength. This process is repeated for multiple stress levels to define a strength envelope (Figure 4-3). All specimens were saturated.

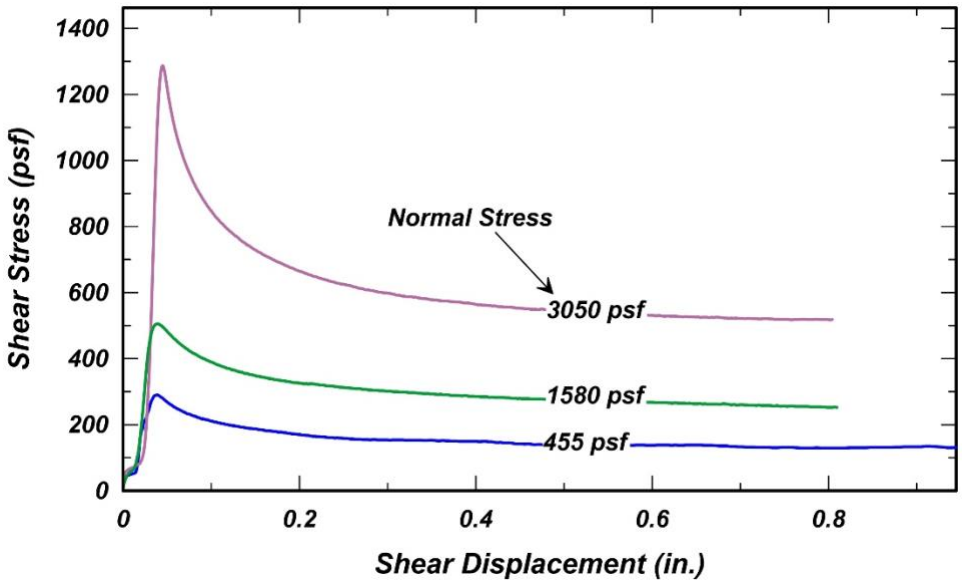

Figure 4-2: Shear stress versus displacement curves for three ring shear tests performed on samples from SR-5 at normal stresses of 455, 1,580 and 3,050 psf, respectively.

The fully softened and residual strengths from the six sites tested in this study are shown in Figure 4-3 for the full range of stresses considered, while results for stresses less than 3200 psf in Figure 4-4. The individual test results are shown along with a power fit envelope. There is scatter within each of the data sets, but some trends are visible. The data from I-65 has the lowest fully softened strength and residual strengths, followed by SR-5 and I-59. SR-22 and SR-219 have similar fully softened strengths to SR-5, but do not experience the same level of softening. The samples from US-231 stands out again as unique. At low stresses (below 1000 psf), US-231 has the highest fully softened and residual strengths. At higher stresses, the residual strength envelope becomes very curved as the soil undergoes significant softening and the residual strength becomes

similar to the soils tested from I-59. This significant level of softening may explain some of the stability problems observed in similar soils in other regions.

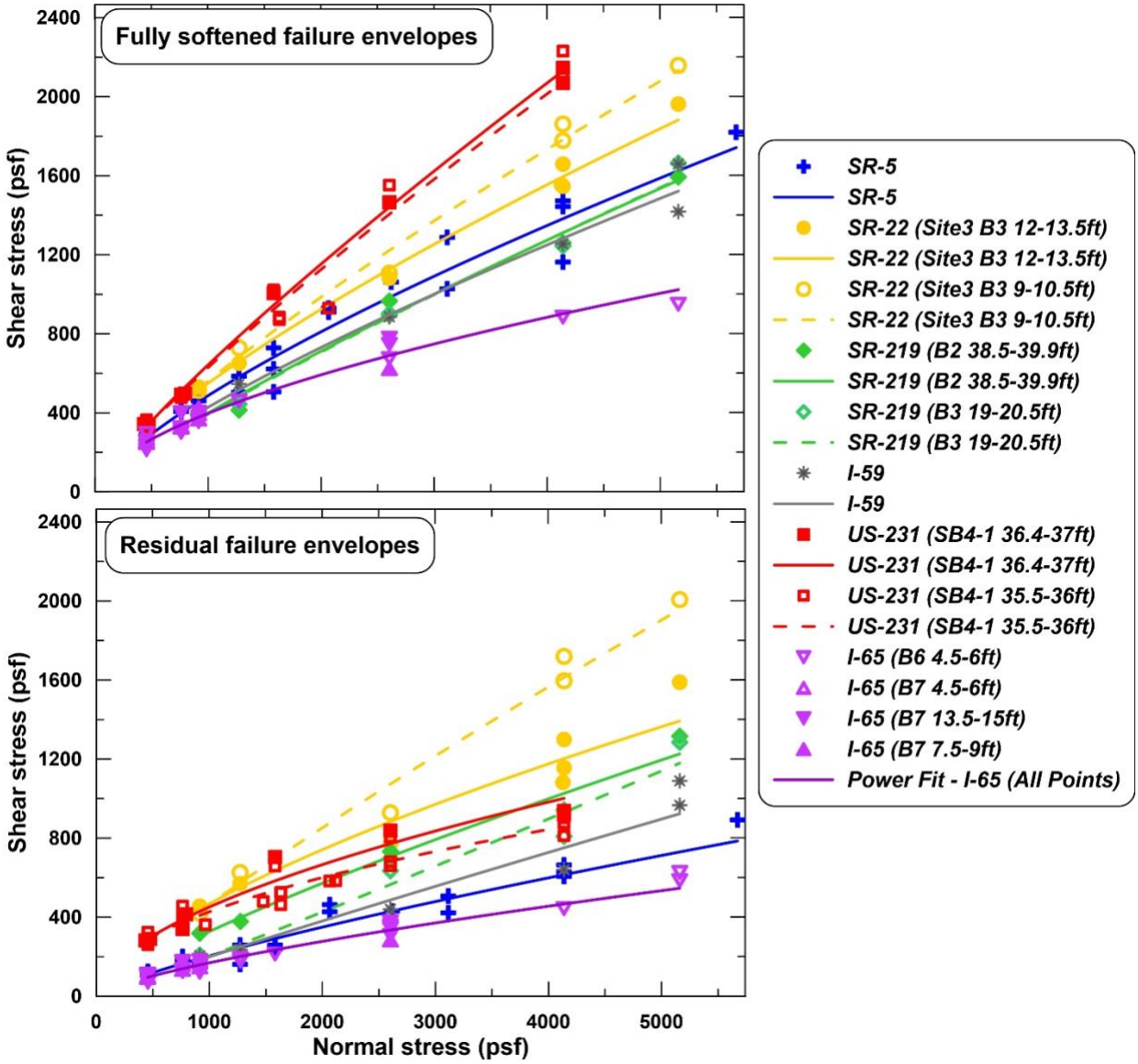

Figure 4-3: Saturated residual and fully softened shear strengths from ring shear tests performed on clay samples collected for this study over the full range of normal stresses.

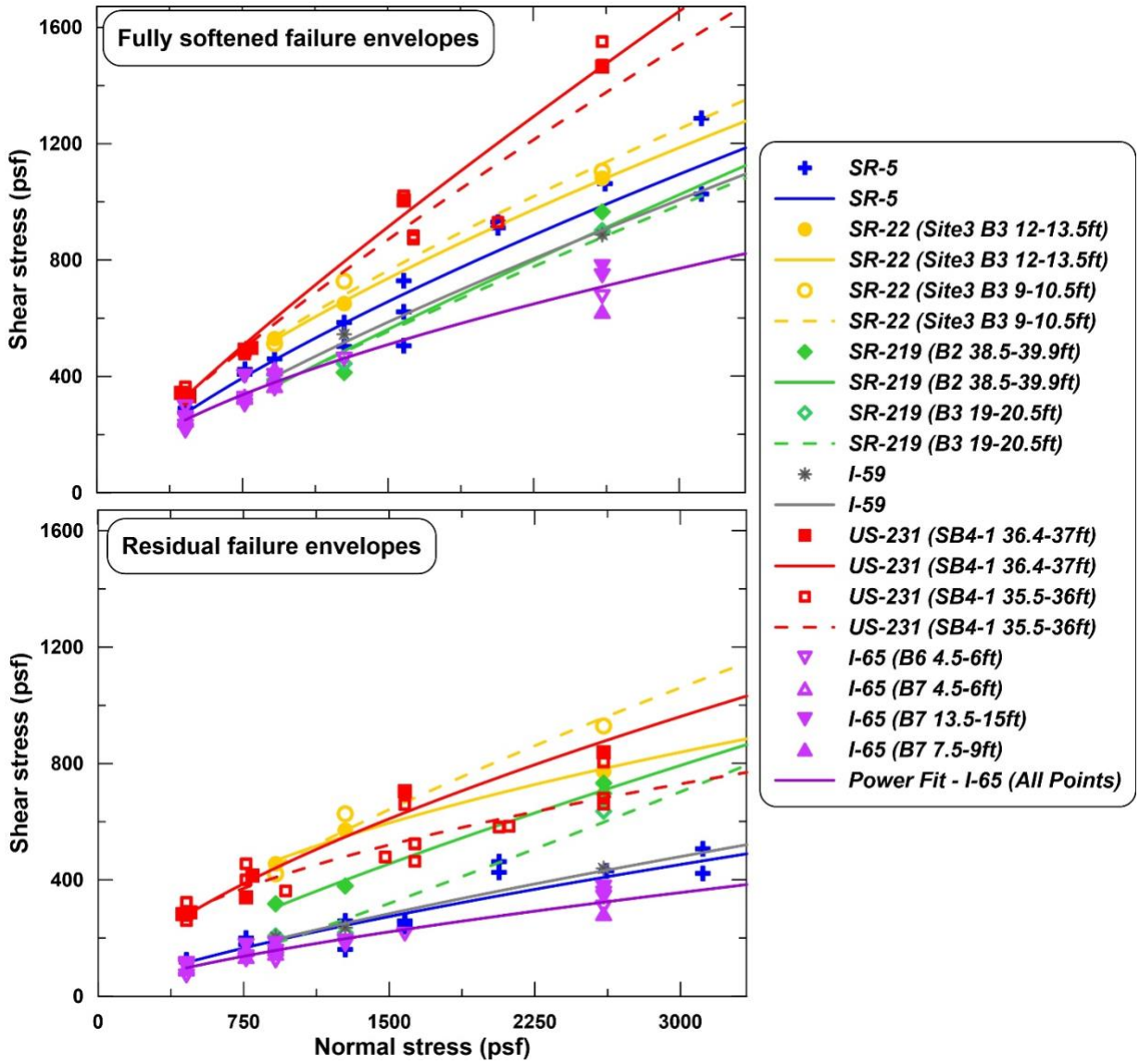

Figure 4-4: Saturated residual and fully softened shear strengths from ring shear tests performed on clay samples collected for this study for stresses less than 3200 psf (approximately 1.5 bar).

The strength envelopes for US-231 were quite different from the other samples, so a comparison was made with strength tests performed by Okagbue (1986) on a similar red shale from West Virginia (Figure 4-5). The index properties and XRD results of the soil tested by Okagbue (1986) were similar to the soils from US-231. Okagbue (1986) performed direct shear tests on intact samples of the shale collected from the interface between a spoil pile and natural ground. The effective stresses used in the direct shear tests are not reported in the paper, but the slide plane was located at a depth of 15 – 30 feet in the central portion of the slide. The water table depth was also located at depth of approximately 15 feet in the analysis. This would suggest

effective stresses between 1,000 and 2,500 psf would be a reasonable range for testing. The peak strength envelopes measured by Okagbue (1986) were higher than the fully softened envelope measured in this study, but this is expected as Okagbue (1986) tested intact instead of remolded specimens. The residual strength envelopes are also higher than those measured in this study, but the difference is not significant at stresses below 1,500 psf. It is interesting that the envelope used in the back-analysis is in good agreement with the ring shear tests between 1,000 and 2,000 psf.

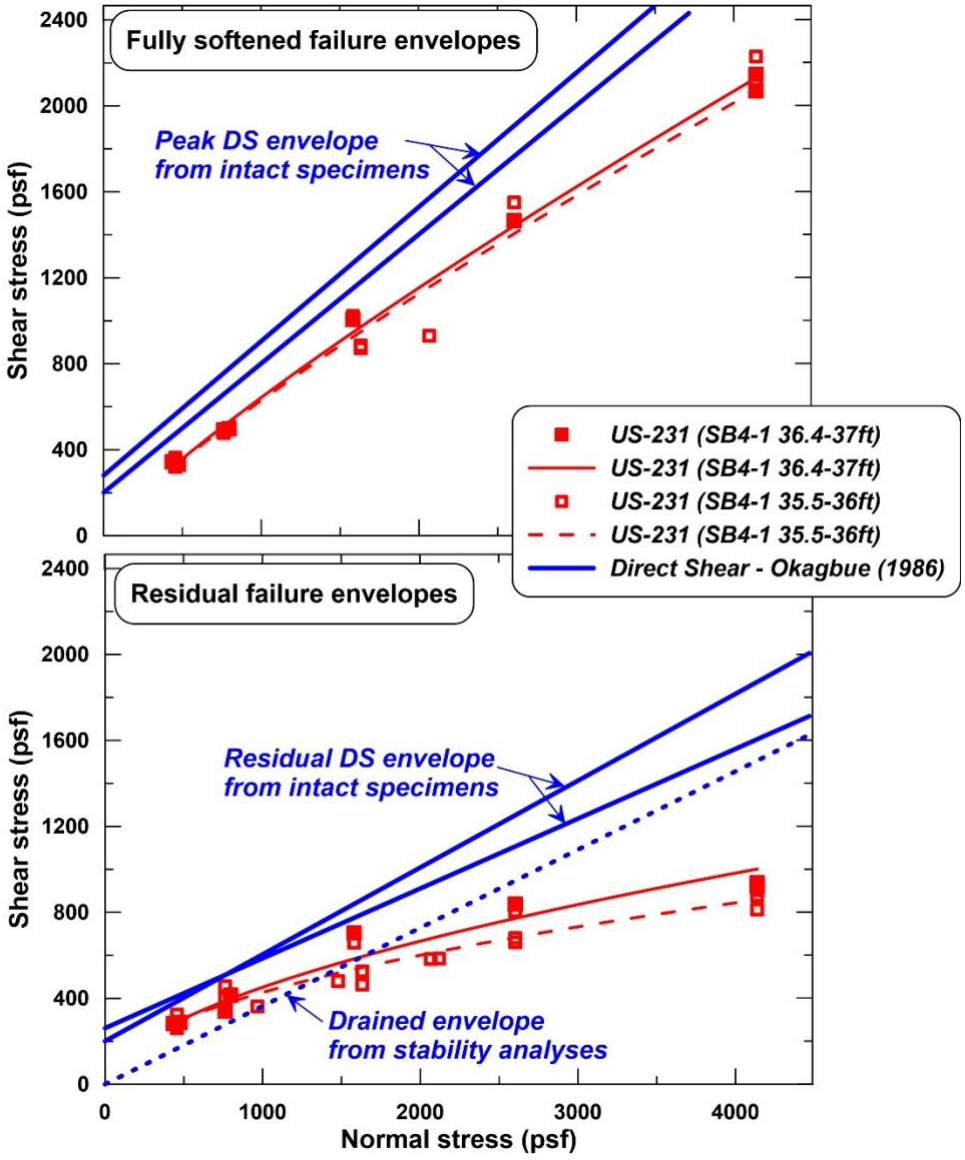

Figure 4-5: Saturated residual and fully softened shear strengths from ring shear tests performed on clay samples from US-231 compared with strength results from Okagbue (1986). Okagbue (1986) performed direct shear (DS) tests on two intact samples of red shale collected from a landslide site in West Virginia. The strength envelope used by Okagbue (1986) for back-analysis is also shown for comparison.

The comparison between the ring shear results and the strength envelopes from Okagbue (1986) highlight the need to consider stress-dependent strength envelopes for these soils. The true strength envelope is curved with a decreasing slope (i.e., friction angle) as effective stress increases. Over a limited stress range this can be reasonably approximated as a straight line, but care must be taken to ensure that the strength tests are performed at similar effective stresses to those used in the analyses. The comparison of the strength envelopes in Figure 4-5 clearly demonstrates this. The linear envelope used for back-analysis by Okagbue (1986) would be a good match to the strength data measured in this study between 1,000 and 2,000 psf but would underestimate strengths at lower stresses and overestimate strengths at higher stresses. Using a nonlinear envelope like the power function shown in Figure 4-5 or a secant friction angle relationship would allow a single envelope to be used over a much wider range of stresses.

4.4 Comparison with Existing Correlations

The data presented in Figure 4-3 are only applicable to the sites and depths where measurements were conducted. To be applicable to other sites, correlations must be developed based on the properties of the samples. The database developed in this study is too limited to develop new correlations, but it is sufficient to examine previously developed correlations and to identify which would be most applicable to clays in Alabama.

As part of this study, a thorough literature review was performed to identify correlations for both fully softened and residual shear strengths that properly accounted for the curved strength envelopes observed in Figure 4-3. are compared separately with five correlations that relate the shear strength to soil index properties. Eight fully softened strength (FSS) correlations from Mesri and Shahien (2003) (upper, middle, and lower bound relationships), Wright (2005), Stark and Hussain (2013), Eid and Rabie (2017), Stark and Fernandez (2020), and Stark (2022) were selected for comparison. These are referred to as “FSS models” in the following sections and comparisons between the data and models are made in terms of the secant friction angle at each stress level. Eight residual strength (RS) correlations from Mesri and Shahien (2003) (upper, middle, and lower bound relationships), Wright (2005), Stark and Hussain (2013), Eid et al. (2016) (CF and LL, and PI relationships), and Stark and Idries (2021) as implemented by Stark (2022) were selected and will be referred to as “RS models”. Wright (2005), Eid et al. (2016), Eid and Rabie (2017), and Stark and Fernandez (2020) provided equations that correlated the strength of the soil to the clay fraction, LL, and/or PI as a function of effective stress. Wright (2005) uses equations developed

by Stark (2005) for clay fractions less than 50% and so is listed as Wright/Stark (2005) in the comparisons. These equations were used to compute the model strength for each test considering the index properties from Chapter 3 and the stress level of the test. Stark (2022) provides a spreadsheet that correlates the power function parameters to the liquid limit and clay fraction of the soil and these parameters were used to calculate strengths at each stress level. Stark and Hussain (2013) and Mesri and Shahien (2003) provide relationships that estimate the strength at discrete stress levels, so a power function was fit to the individual points from each of these correlations in order to develop strength estimates over the full range of stresses tested in this study. A separate power function was fit for each correlation and each soil sample due to differences in the index properties. Additional details are discussed by Xuan (2023).

The data and models were compared by calculating residuals based on the measured and predicted secant friction angles (Residual = $[\phi'_{sec}]_{data}$ - $[\phi'_{sec}]_{model}$). The secant friction angle was computed by taking the inverse tangent of the shear strength divided by the normal stress for each test. Using this definition, a negative residual indicates that the model (correlation) is overpredicting the strength relative to the measurements. Summaries of the root mean square (RMS) residual and average residual for the FSS models are shown in Table 4-1 and for the RS models in Table 4-2. Based on the overall results, thresholds of 3.0 degrees for the RMS residual and $\pm$1.5 degrees for the average residual were selected to define good agreement. The models meeting both of these criteria are highlighted in the tables.

For the FSS strengths, almost all of the models are overpredicting strengths for SR-22, SR-219, and I-59. Stark and Idries (2021) is the closest fit for these sites, but still overpredicts by an average of 3 – 9 degrees except for the shallower SR-22 sample, which is well fit. For the other sites, Stark (2022), Stark and Hussain (2013), Wright/Stark (2005), and the lower bound of Mesri and Shahien (2003) also provide the best agreement with the average difference being less than two degrees for most of the sites. This level of agreement is well within the scatter of the data.

For the residual strengths, most of the models are also overpredicting the measured strengths for SR-219, I-59, and US-231. Wright/Stark (2005) is the closest for these three sites, but there is significant scatter. For the other sites, Stark (2022), the LL-based relationship from Eid et al. (2016), Stark and Hussain (2013) and Wright/Stark (2005) provided the best fit, but the level agreement is a little worse than it was for the FSS strengths. The lower bound relationship from Mesri and Shahien (2003) is also in reasonable agreement, but tends to underestimate RS.

Table 4-1: Comparisons between the fully softened shear strength data and models. The residuals are computed as the difference between the secant friction angle measured in the experiment and the secant friction angle predicted by the model. The root mean square (RMS) residual and average residual are computed for each model. A negative average residual indicates the model is overpredicting the strength. Models with an RMS residual less than 3.5 degrees and an average residual less than ±1.5 degrees are highlighted.

Site	Boring	Depth Range (ft)	Mesri and Shahien (2003) - Upper		Mesri and Shahien (2003) - Middle		Mesri and Shahien (2003) - Lower		Wright/Stark (2005)	
			RMS Residual	Average Residual	RMS Residual	Average Residual	RMS Residual	Average Residual	RMS Residual	Average Residual
SR-5	B-5.5A	1-7	6.28	-5.21	3.98	-2.52	2.78	-0.53	3.06	-0.34
SR-22	B-3	12-13.5	10.91	-10.42	6.75	-6.32	4.43	-3.87	5.36	-5.04
SR-22	B-3	9-10.5	7.89	-7.49	4.22	-3.77	1.95	-1.09	3.29	-2.91
SR-219	B-2	38.5-39.9	14.43	-14.25	10.61	-10.46	6.83	-6.42	9.81	-9.67
SR-219	B-3	19-20.5	13.52	-13.43	9.84	-9.78	7.40	-7.32	7.60	-7.53
I-59	B-1	33.5-35	13.16	-12.95	9.24	-9.08	6.86	-6.71	5.49	-5.33
US-231	SB4-1	35.5-36	4.47	-2.80	2.47	0.22	4.15	2.59	1.97	1.17
US-231	SB4-1	36.4-37	4.48	-2.49	2.78	0.28	4.37	2.83	2.60	1.00
I-65	B-6	4.5-6	10.05	-9.27	7.42	-6.62	5.62	-4.94	4.28	-2.87
I-65	B-7	4.5-6	4.88	-4.41	2.95	-2.25	1.88	-0.74	2.06	0.81
I-65	B-7	7.5-9	7.18	-6.03	5.10	-3.83	3.63	-2.02	3.28	0.06
I-65	B-7	13.5-15	11.43	-10.94	8.82	-8.32	6.86	-6.38	4.95	-4.06

Site	Boring	Depth Range (ft)	Stark and Hussein (2013)		Eid and Rabie (2017)		Stark and Fernandez (2020)		Stark (2022) - LL	
			RMS Residual	Average Residual	RMS Residual	RMS Residual	Average Residual	Average Residual	RMS Residual	Average Residual
SR-5	B-5.5A	1-7	2.61	-0.16	3.67	-1.73	3.18	-0.97	3.26	1.41
SR-22	B-3	12-13.5	5.24	-4.92	7.05	-6.54	5.29	-4.73	4.99	-4.37
SR-22	B-3	9-10.5	3.20	-2.83	4.26	-3.71	2.57	-1.79	1.92	0.54
SR-219	B-2	38.5-39.9	9.73	-9.59	10.64	-10.46	8.82	-8.64	9.07	-8.89
SR-219	B-3	19-20.5	6.37	-6.27	10.47	-10.38	8.63	-8.54	5.34	-5.23
I-59	B-1	33.5-35	4.62	-4.50	9.38	-9.19	7.43	-7.25	3.55	-3.29
US-231	SB4-1	35.5-36	2.00	1.24	2.66	0.35	2.83	1.65	3.44	2.57
US-231	SB4-1	36.4-37	2.40	0.74	3.06	0.44	3.30	1.81	3.56	2.19
I-65	B-6	4.5-6	3.96	-3.08	6.93	-6.01	6.32	-5.49	3.44	-1.50
I-65	B-7	4.5-6	1.60	0.08	2.45	-1.49	2.14	-1.10	2.85	2.22
I-65	B-7	7.5-9	2.73	-0.36	4.70	-3.13	4.05	-2.41	3.49	1.51
I-65	B-7	13.5-15	5.23	-4.65	8.19	-7.60	7.40	-6.84	3.80	-2.58

Table 4-2: Comparisons between the residual shear strength data and models. The residuals are computed as the difference between the secant friction angle measured in the experiment and the secant friction angle predicted by the model. The root mean square (RMS) residual and average residual are computed for each model. A negative average residual indicates the model is overpredicting the strength. Models with an RMS residual less than 3.5 degrees and an average residual less than ±1.5 degrees are highlighted.

Site	Boring	Depth Range (ft)	Mesri and Shahien (2003) - Upper		Mesri and Shahien (2003) - Middle		Mesri and Shahien (2003) - Lower		Wright/Stark (2005)	
			RMS Residual	Average Residual	RMS Residual	Average Residual	RMS Residual	Average Residual	RMS Residual	Average Residual
SR-5	B-5.5A	1-7	4.24	-3.83	1.76	-0.51	2.07	0.99	2.14	-1.06
SR-22	B-3	12-13.5	8.59	-7.52	4.06	-1.80	4.15	1.62	2.91	-1.42
SR-22	B-3	9-10.5	2.64	-1.70	4.36	4.03	7.53	7.30	3.13	2.73
SR-219	B-2	38.5-39.9	11.68	-11.65	4.49	-4.30	1.71	-0.88	5.64	-5.59
SR-219	B-3	19-20.5	11.59	-11.38	6.40	-5.85	3.67	-2.80	3.31	2.98
I-59	B-1	33.5-35	11.95	-11.89	7.70	-7.55	4.58	-4.39	3.20	-2.94
US-231	SB4-1	35.5-36	8.11	-5.32	6.65	0.17	8.01	3.92	4.73	-0.17
US-231	SB4-1	36.4-37	9.00	-5.69	7.03	-0.55	7.87	3.07	5.36	0.52
I-65	B-6	4.5-6	3.18	-5.38	2.78	-2.50	1.60	-0.63	1.51	-0.56
I-65	B-7	4.5-6	4.26	-4.22	1.37	-1.23	1.25	1.07	0.63	0.07
I-65	B-7	7.5-9	5.45	-5.29	5.45	-5.29	1.49	0.34	1.44	0.29
I-65	B-7	13.5-15	6.98	-6.94	3.60	-3.57	2.01	-1.84	1.54	-1.33

Site	Boring	Depth Range (ft)	Stark and Hussein (2013)		Eid et al. (2016) - LL		Eid et al. (2016) - PI		Stark (2022) - LL	
			RMS Residual	Average Residual	RMS Residual	RMS Residual	Average Residual	Average Residual	RMS Residual	Average Residual
SR-5	B-5.5A	1-7	1.99	-1.21	1.98	-1.10	1.90	-0.83	1.97	-1.18
SR-22	B-3	12-13.5	4.57	-3.74	4.93	-3.18	4.77	-3.00	4.03	-2.96
SR-22	B-3	9-10.5	1.58	0.44	2.20	1.12	3.31	2.78	1.96	1.26
SR-219	B-2	38.5-39.9	7.89	-7.85	7.13	-6.96	5.70	-5.51	7.09	-7.05
SR-219	B-3	19-20.5	6.29	-5.76	2.82	2.13	8.67	-8.45	6.24	-5.71
I-59	B-1	33.5-35	3.99	-3.63	8.99	8.90	7.65	-7.55	3.98	-3.62
US-231	SB4-1	35.5-36	5.41	-2.30	6.70	-0.13	6.78	-0.91	5.25	-1.38
US-231	SB4-1	36.4-37	6.93	-4.08	7.48	-1.98	7.35	-1.69	6.57	-3.17
I-65	B-6	4.5-6	1.50	-0.90	1.54	-0.86	3.02	-2.75	1.48	-0.86
I-65	B-7	4.5-6	0.89	-0.65	0.69	-0.35	1.77	-1.67	0.84	-0.57
I-65	B-7	7.5-9	1.04	-0.08	1.17	0.05	2.71	-2.43	1.05	-0.01
I-65	B-7	13.5-15	2.09	-2.06	1.64	-1.51	3.99	-3.95	1.52	-1.44

From the results shown in Table 4-1 and Table 4-2, the lower bound relationships from Mesri and Shahein (2003), the relationships from Wright (2005) with the additional equations from Stark (2005) and the LL-based relationship from Stark (2022) were selected for further examination. These relationships were selected as they provide both fully softened and residual strength estimates and had some of the lowest residuals across the range of sites. To examine potential bias in the results, residuals from the three best correlations were plotted versus effective stress and liquid limit, which serves as an input for all three models. The results are shown in Figure 4-6, Figure 4-7, and Figure 4-8. These figures show that all three models overestimate the fully softened strengths for SR-219, SR-22, and I-59 regardless of stress level. This does create a bias within the residuals with respect to the liquid limit. The residuals also show a bias with respect to effective stress with the models tending to underpredict the strength at low effective stresses and overpredict strength at higher stresses. This is more apparent for the fully softened strengths than for the residual strengths. It is worth noting that the databases used to create these relationships were primarily created based on results from west of the Mississippi and so may not be capturing the curvature of older clays like those in Alabama.

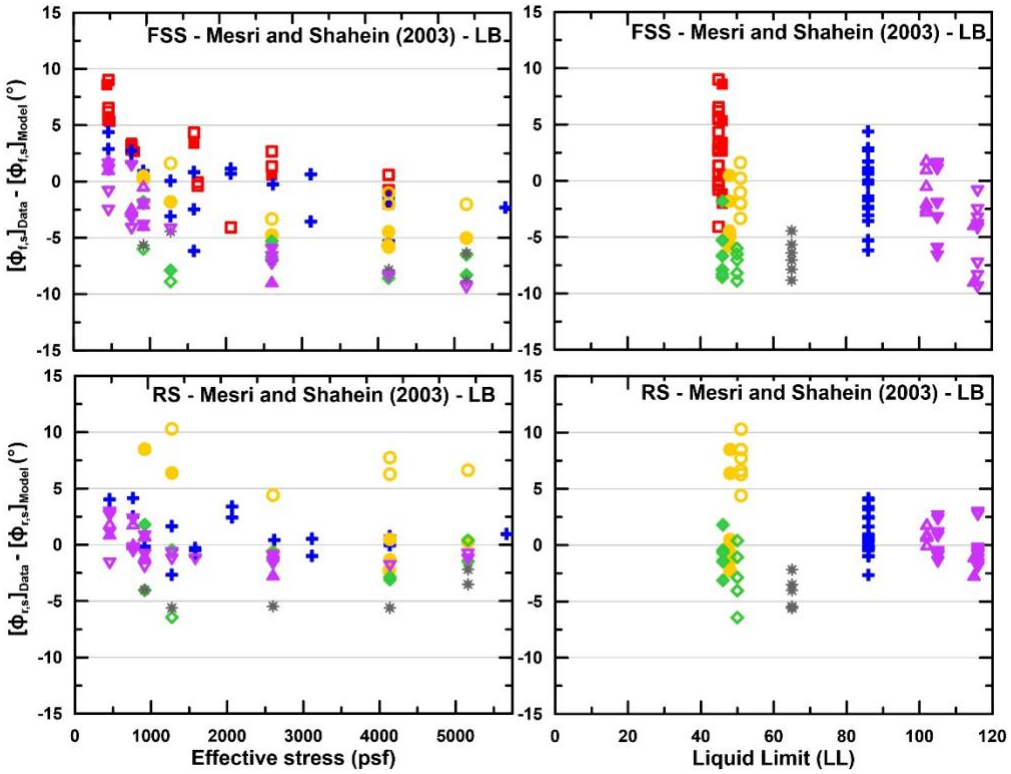

Figure 4-6: Residuals (data – model) for fully softened and residual secant friction angles predicted by the lower bound relationship from Mesri and Shahein (2003).

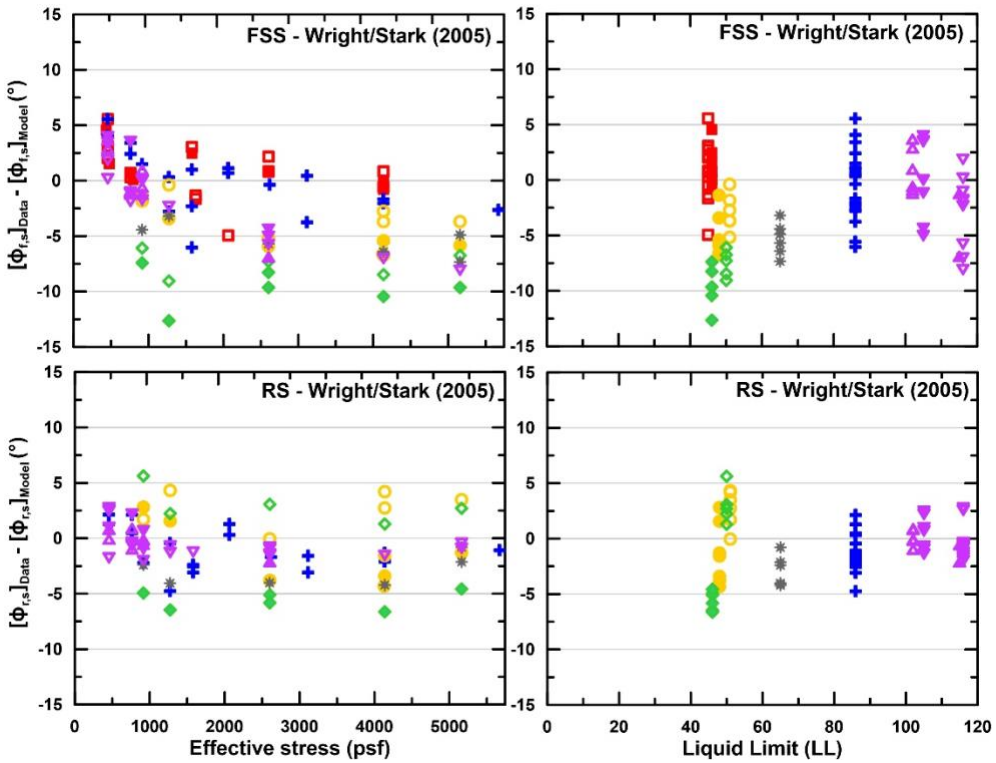

Figure 4-7: Residuals (data – model) for fully softened and residual secant friction angles predicted by the relationships from Wright (2005), which include equations from Stark (2005).

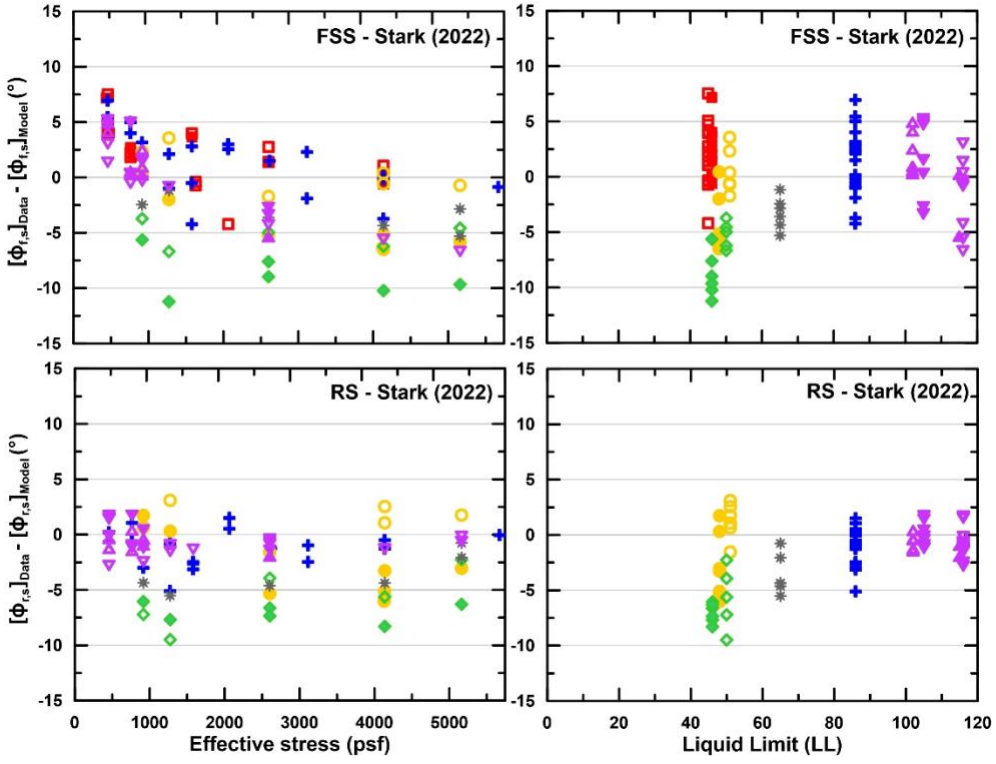

Figure 4-8: Residuals (data – model) for fully softened and residual secant friction angles predicted by the spreadsheet provided by Stark (2022).

The residual strength for US-231 was not fit well by any of the correlations due to the large curvature in the envelope (Figure 4-5). This unique behavior is believed to be a function on the mineralogy of this soil and similar soils (i.e., degraded illites from Ohio, Pennsylvania, West Virginia, Alabama) do not appear to have been included in previous databases used to develop these correlations. This study is believed to be the only one to perform ring shear tests on these samples, so there is some uncertainty in the strength characterization. Wu et al. (1987) examined stability of slopes with red Round Knob and Connesville shales in eastern Ohio and performed direct shear tests on samples with slickensides to obtain the residual strength. These shales have LLs between 30 and 48 and PIs between 10 and 22 (Wu et al. 1993), which covers the range observed at US-231. Wu et al. found that using a residual friction angle of 14 degrees provided a reasonable fit to their tests. This is lower than the 22 degrees determined by Okagbue (1986), but Okagbue was focused on shallower slides and the friction angle is expected to increase at lower effective stresses. The results from the direct shear tests are compared with the ring shear results from this study in Figure 4-9. The tests are in very good agreement for stress levels between 2000 psf and 4000 psf with the slickensides showing a more linear envelope. Overall, these results give additional confidence in the reasonableness of the measured results from US-231, which largely fall between the friction angles estimated in previous studies.

As the measured results from US-231 are in reasonable agreement with the tests from Wu et al. (1987), an effort was made to determine how the correlations from Stark (2022) might be modified to fit the US 231 data. The curvature of the envelope for US-231 is outside the bounds of the database examined by Stark and Idries (2021), so two curves were fit to provide bounds on the measured data. The first curve uses the LL of the site (45) and the measured clay fraction (40.9%), while the second curve uses a LL of 90 to provide a lower bound on the data. Both curves are shown for residual and fully softened strengths in Figure 4-9. The fully softened curve using the true material properties provides a good fit to the measured data, while the curve using a LL of 90 underestimates the measured strengths. For the residual strengths, the two curves provide excellent bounds for the data from US-231 and the strength envelopes from Okagbue (1986) and Wu et al. (1987). Additional data is needed to determine if new correlations should be developed to fit soils similar to those found at US-231, but the residual strength bounds shown in Figure 4-9 should be reasonable to use for stability analyses in similar soils.

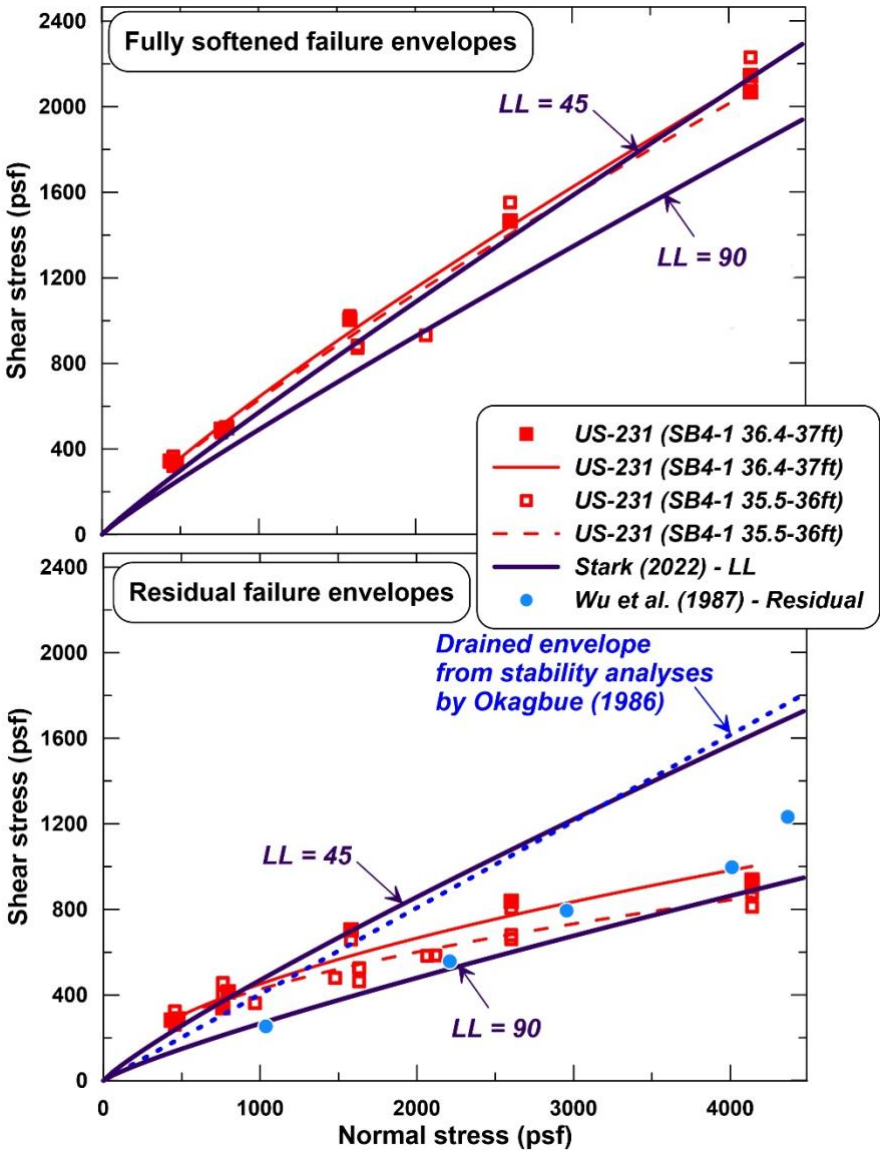

Figure 4-9: Comparison of fully softened and residual strength envelopes measured at US-231 with envelopes predicted by the spreadsheet provided by Stark (2022) and used by Okagbue (1986) for back analysis of a slope failure in similar soils. Direct shear results by Wu et al. (1987) from slickensides found within red shale deposits in western Ohio are shown for comparison.

4.5 Summary

Strengths of clay samples collected at sites in west and north Alabama were measured using ring shear testing. The measured strengths were compared with existing correlations and the correlations implemented by Stark (2022) were found to provide a reasonable fit (secant friction angles within 5 degrees) to the measured data with the exception of residual strengths for US-231. The measured residual strengths from this study were similar to those measured by Wu et al. (1987)

using direct shear tests on slickensides in red shale in western Ohio. Given the agreement between these two different studies using two different test methods (direct shear on slickensides and ring shear on remolded samples), the measured strength envelopes are believed to be accurate, and the correlations do not seem to be capturing the true strength of these soils. A set of strength bounds was shown in Figure 4-9 that can reasonably be used for similar soils until additional test data is available to assess the need for new correlations.

CHAPTER 5: SLOPE STABILITY ANALYSES

5.1 Introduction

To demonstrate the use of the FSS and RS envelopes developed in the previous section, slope stability analyses were performed for SR-5, US-231, and I-65. These three sites were selected as they represented a site without slope failures (SR-5), a site with a significant slope failure (US-231), and a site with a long history of movement (I-65). The measured strength envelopes should be able to distinguish between these three cases if they are going to applied to future analyses. These analyses were performed using both linear and nonlinear strength envelopes to highlight situations where consideration of nonlinear envelopes may be important. Fully softened drained shear strength is investigated first to determine if they the initial failure could have occurred under drained conditions. Peak undrained shear strengths are examined next to investigate the possibility of an initial undrained failure. Residual drained strengths are then examined to estimate stability of the slope on a pre-existing shear surface.

Slope stability analyses are performed using limit equilibrium analyses in Slide (Rocscience 2021) with either circular or noncircular surfaces. The critical circular surfaces are found using an auto-refine search and critical noncircular surfaces are found using an iterative Cuckoo search. All FS values reported for the analyses are calculated using Spencer's method. Nonlinear drained strength envelopes are represented using the power curve option included in Slide. Linear envelopes are represented using the Mohr-Coulomb option and undrained strengths are represented using the vertical stress ratio included in Slide.

5.2 Stability Analyses for SR-5

Slope stability analyses were performed to determine the likelihood of slope failure along the analyzed section of SR-5. The research site for this study is located west of Selma, AL in Perry County (Figure 5-1). The highway in this area is generally flat with the surrounding land consisting of wooded areas and farms. Other areas of this highway (SR-5) with the similar soils have experienced slope failures in the past, such as a failure that led to the placement of rockfill berm on an embankment approximately five miles south of the project site. Stallings (2016) observed cracking along the shoulders of the roadway within the study area that was not clearly attributed to swelling and some rutting and bulging was observed along the embankment face. The combination of cracking and bulging led to the hypothesis that slope movements might be occurring within the study area. Jackson (2016) measured moisture contents and suction values

beneath the roadway and found that suction has been present during the duration of the study period (November 2016 – December 2019) and much of the embankment and foundation was saturated, but negative pore pressures were observed in the embankment.

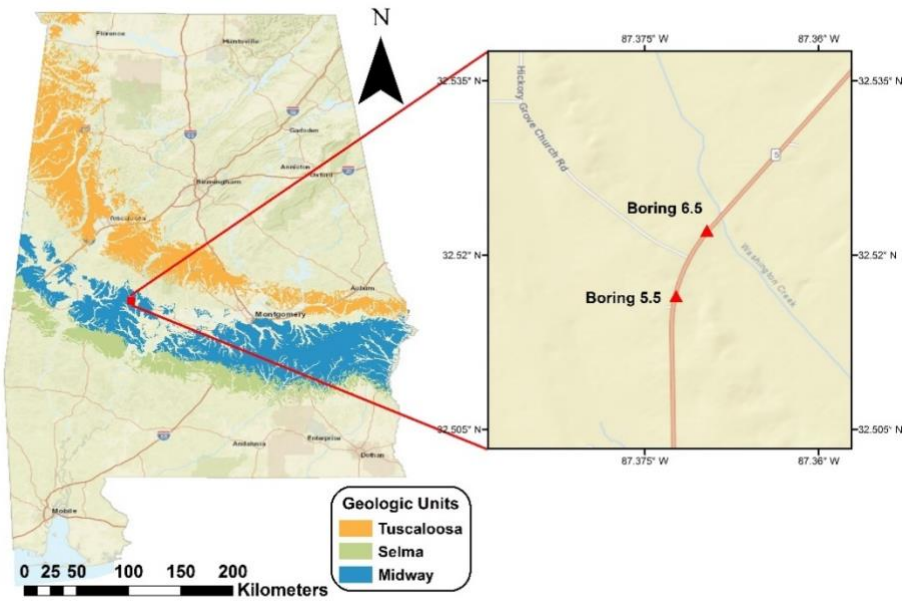

Figure 5-1: Locations of geologic units containing the high plasticity Prairie clays (after Szabo et al. 1988) and the location of the research site and borings examined in the current study.

Analyses were performed using the limit equilibrium slope stability software Slide published by Rocscience (Rocscience 2020). The cross-section near Boring 5.5 was used for the analyses (Figure 5-1) and the soil profiles were obtained from boring logs (Herman 2015, Stallings 2016). The embankment in this area is approximately 5 feet tall and the pavement is relatively thick (1 ft) due to many years of repaving to repair damage from swelling clays. The water table was placed 2.3 ft lower than the embankment for these analyses based on in-situ measurements and field observations. The strength envelopes developed from the ring shear data (Figure 5-3 and

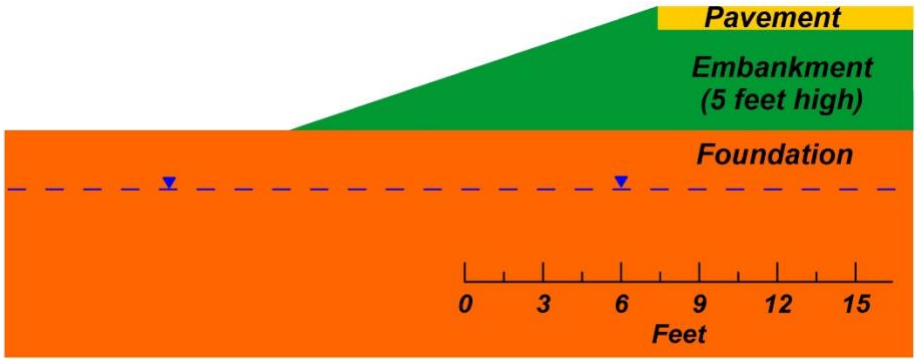

Figure 5-2: Cross-section of SR-5 at borehole B5.5.

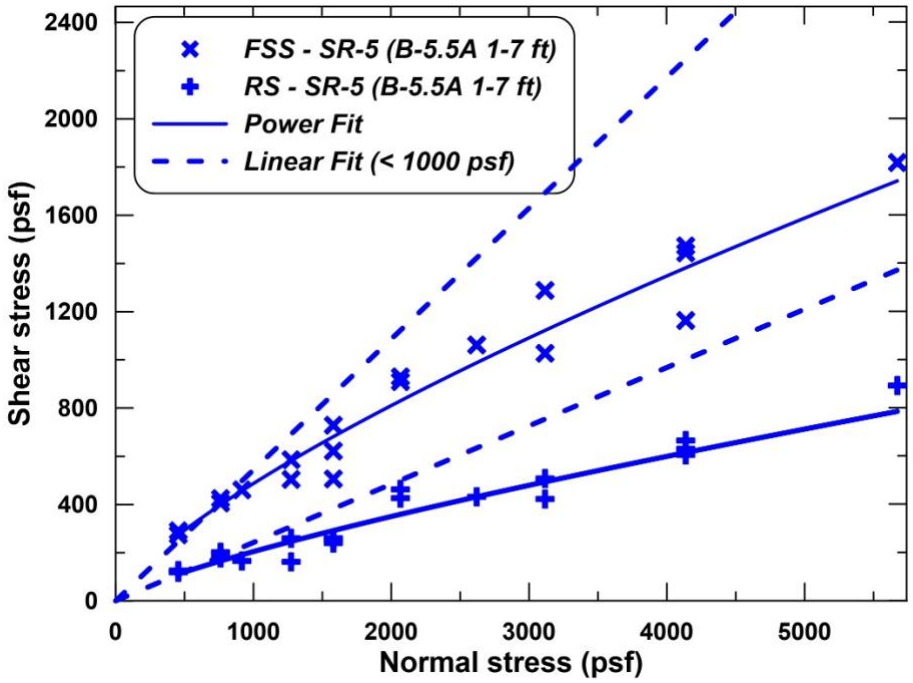

Figure 5-3: Fully softened (FSS) and residual strength (RS) envelopes for SR-5 at borehole B5.5 using both linear fits to data with a normal stress less than 1000 psf and power fits.

Table 5-1) were used to represent the clay embankment and foundation. Strength data for foundation material was the same as embankment. The intact chalk layer (located approximately 6.5 ft below the embankment) was not included in the stability analyses, but no failure surfaces extended to more than 3.3 ft into the foundation. The properties for the pavement (γ = 145 pcf, ϕ = 34°, c = 7700 psf) were based on the lower bound of the triaxial test results presented by Christensen et al. (2000) and the densities of the embankment and the foundation were based on tests performed by Stallings (2016).

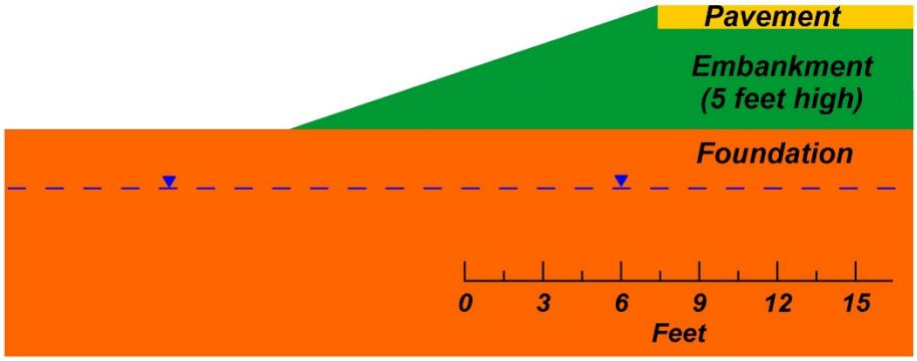

Figure 5-2: Cross-section of SR-5 at borehole B5.5.

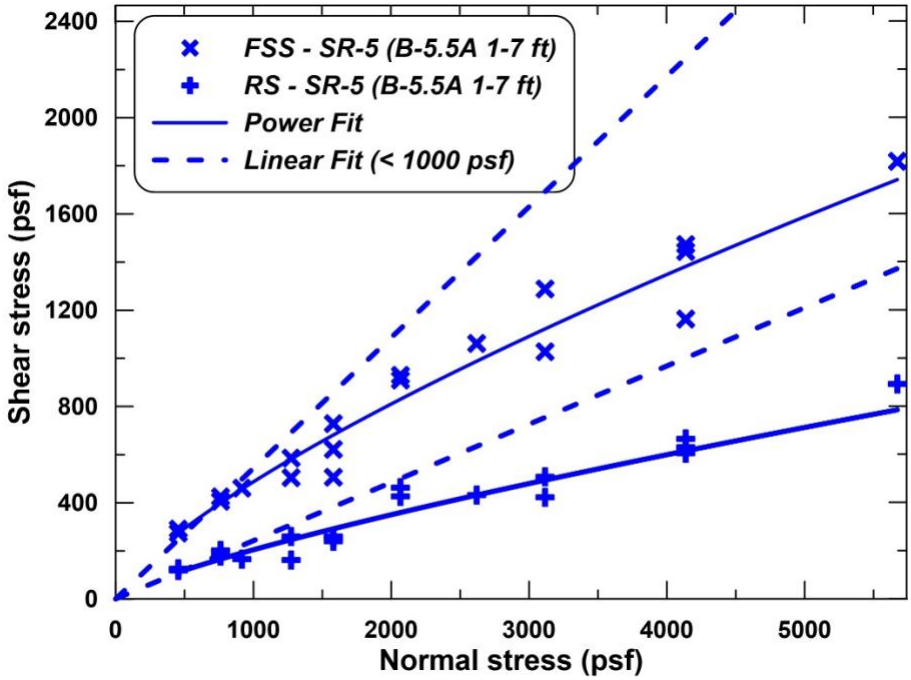

Figure 5-3: Fully softened (FSS) and residual strength (RS) envelopes for SR-5 at borehole B5.5 using both linear fits to data with a normal stress less than 1000 psf and power fits.

Table 5-1: Saturated Shear Strength Envelopes for SR-5

Envelope Types	Strength Envelope (kPa)	R^2
Residual Strength – Linear Fit	$\tau = \sigma' \cdot \tan(13.6°)$	0.98
Residual Strength – Power Fit	$\tau = 0.173 \cdot P_a \left(\frac{\sigma'}{P_a}\right)^{0.75}$	0.88
Fully Softened Strength – Linear Fit	$\tau = \sigma' \cdot \tan(28.5°)$	0.99
Fully Softened Strength – Power Fit	$\tau = 0.407 \cdot P_a \left(\frac{\sigma'}{P_a}\right)^{0.79}$	0.93

The results of the slope stability analyses are shown in Table 5-2. The critical surface for both linear envelopes without suction is very shallow and approximates an infinite slope failure condition. This is not surprising as an infinite slope failure is often the critical case for frictional materials. The slope angle of the embankment is approximately 20 degrees and so the fully softened friction angle gives adequate stability, while the residual strength friction angle shows instability would be expected for an infinite slope failure. The analyses for the residual envelope were re-run with a minimum slice depth of 1.6 ft to examine the stability against larger failures (Figure 5-4). These results still show a factor of safety below 1.0 indicating that larger failures may be expected if these residual strengths are mobilized, and the effects of suction are removed.

The fully softened results, which would be used for first-time slides, indicate that adequate stability would be expected even without suction, so a failure would need to be initiated by some external loading or a significant change in the water table in order to mobilize the residual strengths.

Table 5-2: Summary of Minimum Factors of Safety for the Different Strength Envelopes.

	Factor of Safety			
	Fully Softened Strength - Linear fit	**Fully Softened Strength - Power fit**	**Residual Strength - Linear fit**	**Residual Strength - Power fit**
No suction	1.629	2.344	0.726	1.117
No suction – 1.6 ft minimum depth	1.819	2.344	0.810	1.117
With suction	3.320	-	1.480	-

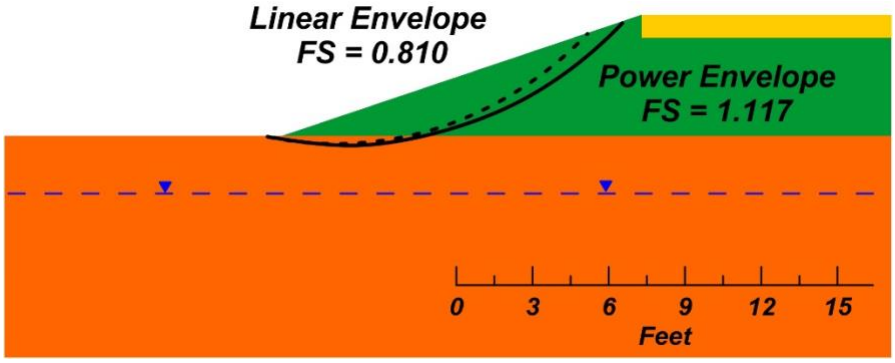

Figure 5-4: Critical failure surfaces for the linear and power fit residual strength envelopes. Similar surfaces were found for the fully softened strengths.

Using the power envelope increases the factors of safety for both strength cases compared with the linear fits. The critical failure surface using the power envelope is similar to the linear case with the minimum depth constraint (Figure 5-4). This difference in factor of safety is due to the higher strengths at very low stresses using the power fit compared with the linear fit. The two envelopes become equal at approximately 500 psf (Figure 5-3) and below this stress level the power envelope gives higher strengths. The differences in the envelopes do not appear to be significant in Figure 5-3, but the effect on the minimum factor of safety is significant, even when considering a minimum depth constraint with the linear envelope. It is important for future studies to recognize that even seemingly small differences in these envelopes can have a significant effect on the results for shallow failures.

Xuan et al. (2021) also explored the effects of suction on the results of these analyses. The details of this analysis are described in the paper, but the results are shown in Table 5-2. Including suction with the linear envelope results in a large increase in the factor of safety as the critical failure surface is pushed farther into the foundation. The factors of safety for the linear envelope with suction are also larger than the results using power fit envelope. This demonstrates the importance of considering reasonable suction profiles when analyzing slopes located above the water table. While designers of new slopes may neglect suction values to avoid relying on them for stability, when analyzing existing slopes, it is important to consider suction conditions as they are likely to exist in the field. For this section of embankment, the stability results do not suggest large failures are likely to occur even if suction is lost.

The results show that under current conditions, both fully softened and residual strength envelopes would indicate stability (factors of safety larger than 1.0) except for the case of a linear residual strength envelope without suction. The linear residual strength envelope indicated that shallow failures would be expected to develop without the effects of suction, but the consideration of suction or the nonlinear envelope removes this concern. This study demonstrates that seemingly small differences in strength envelopes (Figure 5-3) can have a significant effect on the factor of safety for shallow failure surfaces. Neglecting both suction and curvature of the strength envelope could lead to a conclusion that this slope is at risk for failure. This conclusion is at odds with observations at the site and could lead to unnecessary repairs being performed to address stability problems that are unlikely to occur. The consideration of suction or nonlinear strength envelopes indicates the slopes will remain stable even if residual strengths are mobilized.

5.3 Stability Analyses for US-231

Stability analyses were also performed for a large landslide that occurred on US-231 near Laceys Spring, AL on February 13, 2020 following a period of heavy rainfall. The section of highway is a heavily used corridor for Huntsville commuters and closures due to the slide added 30 to 60 minutes to commute times for local residents. This section of highway was likely constructed on an ancient landslide and had a history of movement. Following heavy rain in February 2019, ALDOT drilled five borings and installed inclinometers to monitor slope movement. The rate of movement in the southbound lanes increased following large storms in December 2019 and culminated in the failure of both north and southbound roadway lanes on February 13th (Figure 5-5). On February 14th, Auburn researchers and ALDOT personnel met on

the site and seismic and resistivity tests (Figure 5-6 and Figure 3-11) were performed the following week to better understand the stratigraphy. The consulting firm Dan Brown and Associates was brought in to assist with the slide investigation and design the repair (two bridges with large diameter drilled shaft foundation). The geophysical investigations are described by Montgomery et al. (2021) and the repair is described by Thompson and Dapp (2021).

Borings performed at the site generally show an upper layer of interbedded sand and clay or sandstone and clay, followed by an interbedded clay, mudstone and limestone. The majority of the site is located within the outcrop area of the Pennington Formation, which consists of medium-gray shale, containing interbedded limestone, dolomite, argillaceous sandstone, mudstone, and minor shaly coal (Szabo et al. 1988). Interbedded mudstone and limestone were encountered in all borings at elevations ranging from about 1082 feet to 1087 feet. Above Pennington Formation bedrock, borings showed a mix of fill and colluvium, although it was difficult to identify a clear boundary between these. The inclinometers showed movements were primarily to the north – northwest and at elevations of about 1090-1086 feet in B-2 and about 1094-1088 feet in B-3.

Results from geophysical methods and borings were integrated to identify the stratigraphy at the site. The upper 30 feet of material under both roadways was identified as fill material and colluvium (alternating sandstone and clay), while a low resistivity, low velocity zone was found at depths of 30 – 40 feet below the road. Below this layer, interbedded limestone and mudstone was observed. Based on these observations and the inclinometer data, the likely source of the slide plane was a plastic clay layer found between 30 and 40 feet. Subsequent investigations were able to confirm this layer as the critical zone and characterize the underlying rock for repair design.

Figure 5-5: View of the slide area along US-231 after removal of the pavement. The geophysical survey team can be seen along the SB shoulder on the left side of the figure.

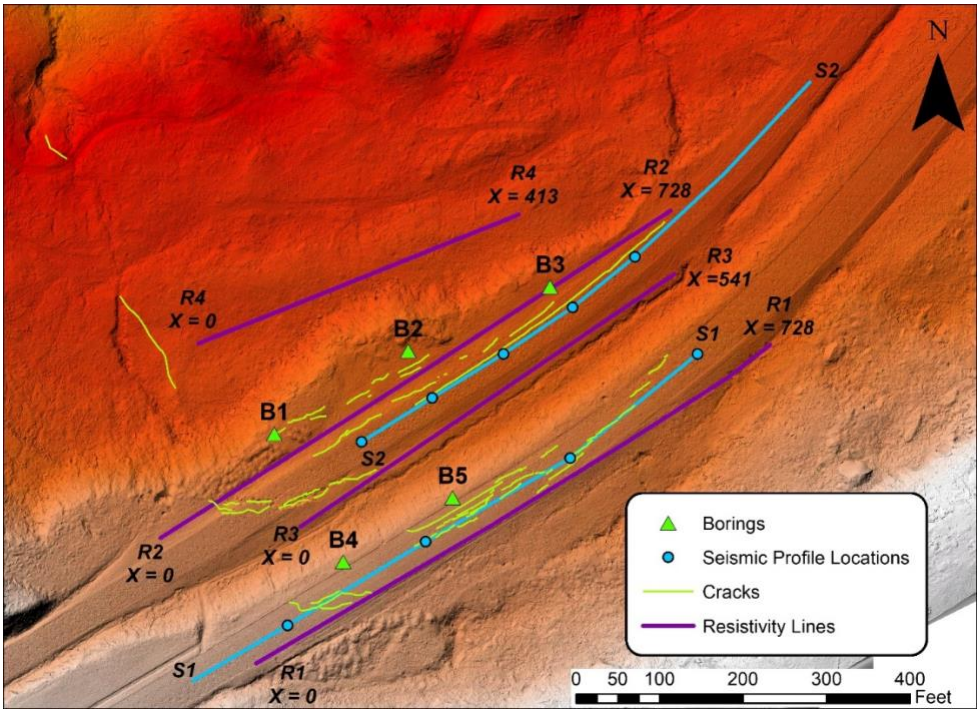

Figure 5-6: Map of the US-231 landslide showing approximate geophysical survey locations along with cracks mapped from UAV images and borings completed by ALDOT. A shaded relief map derived from UAV-based LiDAR collected after the landslide occurred is shown in the background.

Stability analyses were performed using a cross-section (Figure 5-7) through the original roadway near borings B2 and B-5 (Figure 5-6). The tested soil samples were collected from boring SB4-1, which was drilled between B-2 and B-5 along the alignment of the new bridge. The roadway fill was a mix of sandstone and clay and was modeled with a friction angle of 35 degrees and a minor cohesion of 100 psf. The bedrock was considered to be strong and no failure surfaces intercepted the bedrock. The foundation was modeled using the residual strength envelopes shown in Figure 4-9. The power fit for the depth of 35.5 to 36 feet measured in this study was considered along with the two linear envelopes from Wu et al. (1987) and Okagbue (1986), which fit the data from this study at higher and lower stresses, respectively. It is believed that this landslide was due to reactivation of an existing slide plane, so residual strengths are the most accurate to use, but the power fit from the fully softened data was considered as well. The equations for these envelopes are shown in Table 5-3. A minimum depth of 5 feet was used for selecting critical failure surfaces.

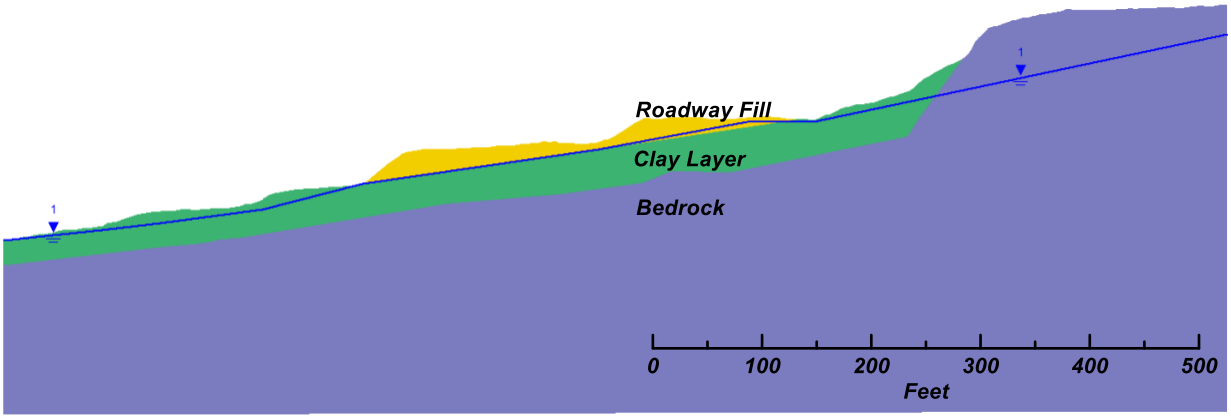

Figure 5-7: Analysis cross-section for US-231.

Table 5-3: Saturated Shear Strength Envelopes for US-231

Envelope Types	Strength Envelope (kPa)	R^2
Residual Strength – Wu et al. (1987)	$\tau = \sigma' \cdot tan(14°)$	N/A
Residual Strength – Power Fit	$\tau = 0.293 \cdot P_a \left(\frac{\sigma'}{P_a}\right)^{0.5}$	0.93
Residual Strength – Okagbue (1986)	$\tau = \sigma' \cdot tan(22°)$	N/A
Fully Softened Strength – Power Fit	$\tau = 0.56 \cdot P_a \left(\frac{\sigma'}{P_a}\right)^{0.89}$	0.98

Two water table levels were considered in the analyses. The first is shown in Figure 5-7 and represents the likely scenario at the time of failure when heavy rain had been occurring in the area and water was ponding on both the upslope and downslope sides of the roadway embankment.

The second scenario considers a water table that is approximately 18 feet below the toe of slope as might be expected during drier weather or with adequate drainage. The factors of safety for these scenarios with the various strength envelopes are shown in Table 5-4: Summary of Minimum Factors of Safety for Southbound Failure for the Different Strength Envelopes.Table 5-4 for the southbound lanes (Figure 5-8). For the FSS, all scenarios have adequate stability. This indicates that without a pre-existing shear plane, the road likely could have remained stable. Unfortunately, the topography suggests an ancient landslide was present in this location and therefore residual strengths should be used. Both circular and noncircular failure surfaces were considered and the results were similar with the noncircular giving slightly lower factors of safety.

Table 5-4: Summary of Minimum Factors of Safety for Southbound Failure for the Different Strength Envelopes.

	Factor of Safety			
	Fully Softened Strength - Power fit	**Residual Strength - Linear fit (22°)**	**Residual Strength - Linear fit (14°)**	**Residual Strength - Power fit**
High GWT – Circular	1.57	1.20	0.80	0.89
Low GWT - Circular	1.89	1.56	1.06	1.01
High GWT - Noncircular	1.44	1.23	0.79	0.81
Low GWT - Noncircular	1.87	1.63	1.06	0.94

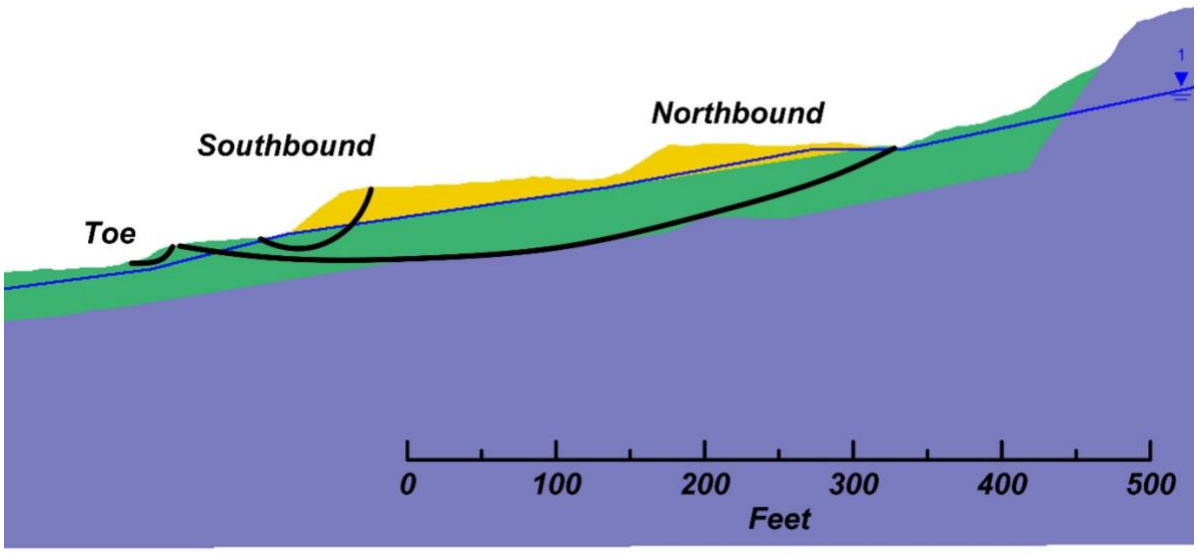

Figure 5-8: Key failure surfaces for US-231. The toe failure circle was only observed when using the linear strength envelopes.

Stability results for the southbound lanes using residual strengths are also shown in Table 5-4. The linear secant envelope for low stress conditions (22 degrees) also shows adequate stability for all scenarios, but a more critical failure surface develops near the toe (Figure 5-8). This surface had factors of safety at or just above 1.0 for this envelope. When the linear envelope is lowered to the high stress condition (14 degrees), the factors of safety for the southbound lanes (where movements began) drop to 0.8 for the higher water table indicating significant movements are likely. For the low water table condition, the factors of safety remain above 1.0, indicating the roadway would likely be stable without the high water table. The factors of safety for the toe circles drop to 0.62 which would suggest widespread slope failures below the roadway. This is not consistent with the observations at the site, as mature trees were present all along the toe of the slope and down the hill with no obvious signs of large failures away from the road. Both circular and noncircular failure surfaces were considered, and the results were very similar.

Results for the power envelope fit to the ring shear data from depths of 35.5 – 36 feet in are shown in Table 5-4 for the southbound lane. The factor of safety for the southbound lanes is below 0.9 for high water levels and near or just below 1.0 for low water tables. This result is consistent with observations at the site, which showed periods of movement and stability until the large rainstorms in 2019 and 2020. The toe circle does not appear in the results using the power envelope as the power envelope gives higher strengths at low stresses. This result demonstrates that the slopes outside of the road area would be stable as observed, while the southbound lanes would become unstable as the water table rose.

The factor of safety for a circle intersecting the northbound lanes (Figure 5-8) was also examined for the high water table conditions. Using the linear envelope with a friction angle of 14 degrees or the power envelope gives a factor of safety of approximately 1.1 for the northbound lanes. This marginal stability indicates that failure would not initiate in the northbound lanes, but movement in these lanes could be triggered once the buttressing effect of the southbound lanes moved. This finding is also consistent with observations as movements were first observed in the southbound lanes with large cracks appearing in 2019 with only minor cracking in the northbound lanes. Similarly, cracking in the southbound lanes led to lane closures on February 11, 2020, while significant movement in the northbound lanes was not observed until the morning of February 13.

5.4 Stability Analyses for I-65

Kiernan (2021) and Kiernan et al. (2022) presented limit equilibrium analyses for the landslide along I-65 in Conecuh County (Figure 5-9). The geophysical investigation for this landslide is also described by Montgomery et al. (2022). This section of the interstate consists of a 7-foot thick compacted clayey sand fill embankment overlying the native soils that consist primarily of high-plasticity clay. The embankment has an average slope angle of 11.7°. The slope angle near the top of the embankment is about 13.8°, and the slope angle near the bottom is about 8.6° (Figure 5-9). The surface geology at the site has been mapped within the Oligocene series undifferentiated geologic unit and generally consists of medium-to-coarse-grained sands; thin-bedded limestone; calcareous and carbonaceous clays; underlain by soft limestone and marl (Szabo et al. 1988; Cook et al. 2004).

A slow-moving landslide is located along the southbound shoulder within the roadway embankment. Persistent cracking has occurred along the southbound shoulder of the roadway over a length of approximately 200 feet, which likely represents the head scarp of the landslide. The location of the landslide toe has not been observed but is thought to be beyond the ALDOT right of way (ROW) that is about 80 feet northwest of the guardrail along the southbound shoulder (roughly along the line connecting borings B5 to B8). While the location of pavement cracking is well defined, the timing of initial movement is uncertain. ALDOT personnel indicate that pavement cracking at the site has been observed as early as 2007. Google Earth images of this location show cracking as far back as 1998, and older Google Earth images make it difficult to determine the presence of cracking due to poor image resolution. It is possible that the initial failure occurred during or after the initial construction of the embankment, which was likely completed in the 1960s or early 1970s, or that pre-existing failure planes were present within the clay at this site.

The drained fully softened and residual strength envelopes obtained from ring shear testing are shown in Figure 4-4. Both a linear fit and a power envelope were examined with the linear envelope resulting in slightly higher factors of safety, but the difference was not significant for this site. This conclusion is different from the two previous analyses, but the clay layer at I-65 is relatively shallow and does not intersect the ground surface, so the surficial failures observed in the previous studies were not critical here.

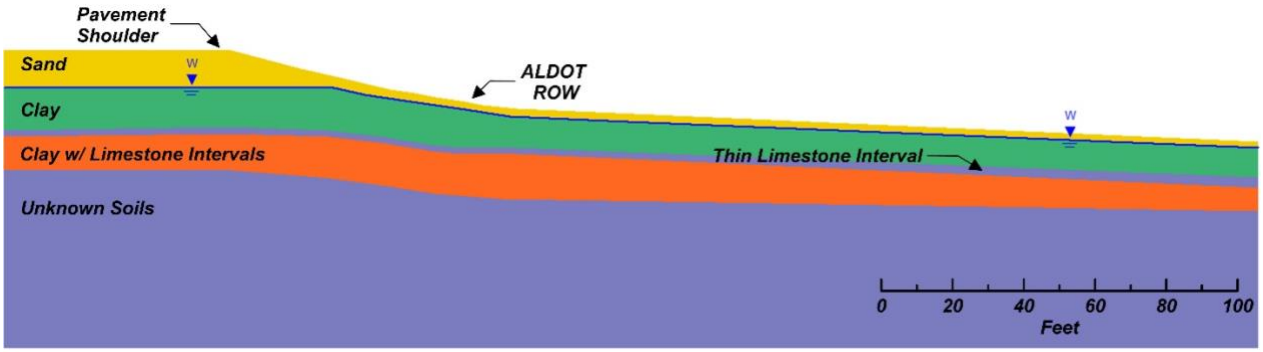

Figure 5-9: Analysis cross-section for I-65 (after Kiernan 2021).

Kiernan et al. (2022) examined by circular and noncircular failure surfaces using limit equilibrium (LEM) analyses in Slide. They found the circular surfaces producing slightly higher factors of safety compared to noncircular. The critical surfaces intersected the roadway just behind the shoulder (Figure 5-10), which is consistent with observed pavement cracking at the site. The surfaces also extended just beyond the ROW, which is also consistent with the lack of bulging within the ROW. Circular surfaces produced shallower failure planes than noncircular surfaces but were generally consistent. The factors of safety for the fully softened strength were approximately 1.5 (Table 5-5) indicating adequate stability against first-time failure. As movements are on-going at the site, residual strengths are more appropriate for analysis and showed factors of safety well below 1.0. Undrained strength analyses were also performed and showed factors of safety at or below 1.0. This indicates that the initial failure at this site may have been due to undrained loading (possibly during initial construction) or the section of roadway may have been built on a pre-existing shear plane.

Table 5-5: Factors of safety for various conditions examined in the slope stability analyses at I-65.

Strength Condition	Factor of Safety: Circular	Factor of Safety: Noncircular
Fully Softened Drained	1.57	1.49
Peak Undrained	0.97	0.91
Residual Drained	0.81	0.71

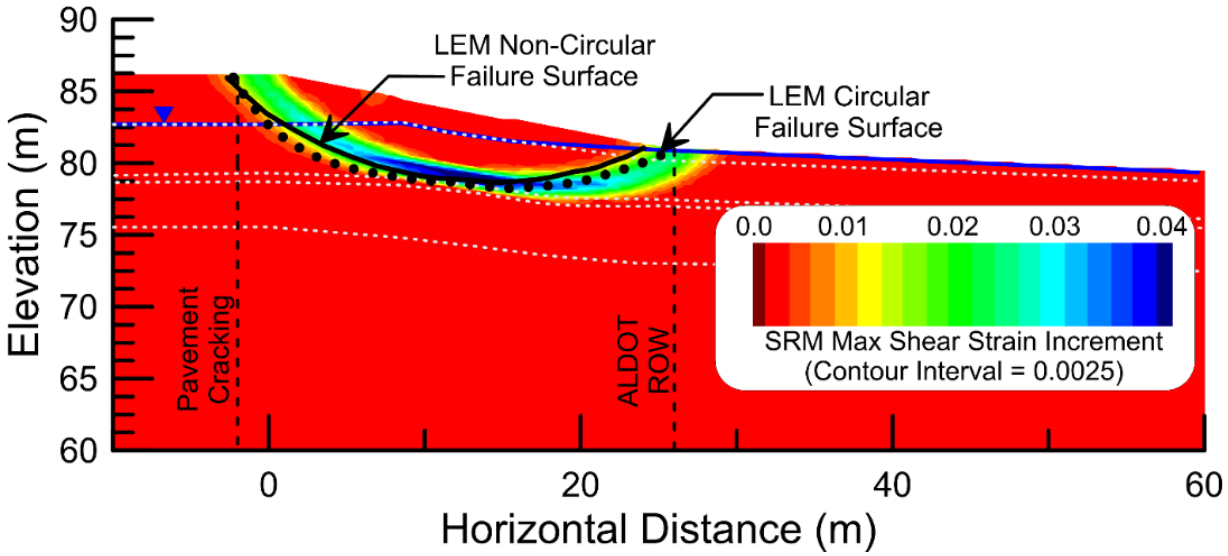

Figure 5-10: Maximum shear strain interval contours (zoomed in on failure surface location) from SRM analysis using fully softened drained strengths with critical noncircular failure surface from LEM shown as solid black line and critical failure surface from LEM with circular surfaces shown by dotted black line. Locations of ALDOT ROW and observed pavement cracking are shown as dashed lines. Soil boundaries (Figure 5-9) are shown by dotted light grey lines.

Kiernan et al. (2022) also compared the results of LEM analyses to analyses using the strength reduction method (SRM). SRM analyses do not require any assumptions on failure surface type or location. The SRM results were very similar to the results using non-circular failure surfaces with FS values within approximately 10%. The noncircular failure planes were also consistent with the critical failure plane locations produced by SRM (Figure 5-10). The comparison of both methods illustrates that LEM and SRM are both valid methods for analyzing slope stability problems. The LEM was much easier to calibrate and analyze and LEM with noncircular failure surfaces was very consistent with SRM results. Using LEM with consideration of both circular and noncircular surfaces is recommended for future analyses.

CHAPTER 6: CONCLUSIONS AND RECOMMENDATIONS

6.1 Summary

Slope failures in clayey soils are a common occurrence in many parts of Alabama. Repairing existing failures and designing new slopes to avoid stability issues requires good characterization of the soil strength. For high plasticity clays, this characterization can be challenging as these soils tend to lose strength during shearing. First-time slides are often analyzed using fully softened strengths to account for potential strength loss due to weathering and changes in moisture content. Once a slide has been mobilized, the strength can drop to a residual value. While fully softened strengths can be analyzed using triaxial and direct shear testing, measuring residual strengths requires tests that can reach large strains.

Ring shear testing can be used to measure how soil strength changes over large displacements. This test is able to measure both the fully softened and residual strength, but its use in practice is limited by the time and effort required to run the test. Correlations for both fully softened and residual strengths have been developed by previous authors, but the databases used to develop these correlations included few if any soils from east of the Mississippi River. The geologic history and mineralogy of the soil will affect its strength, so correlations need to be validated for use in the regions they will be applied.

The current study used ring shear testing to characterize both the fully softened and residual strengths at six sites across the state where clays were thought to be driving stability problems. Clay samples were first characterized using traditional index testing (grain size, Atterberg Limits), X-ray diffraction (XRD) to determine mineralogy, and electrical resistivity to assess the ability of this test to map these soils in the field. Strengths were measured over a wide range of stresses in order to determine whether nonlinear strength envelopes were needed to characterize the soil. The strength results showed that higher plasticity soils like those found at sites along I-65 in Conecuh County and SR-5 in Perry County had the lowest strengths, while medium plasticity clays like those along SR-22 in Chilton County had the highest strengths of the soils examined. Tests from US-231 showed the highest fully softened strength, but the residual strength envelope curved significantly at higher stresses leading to secant friction angles at or below 14 degrees at higher stresses. This seemingly strange result was found to be consistent with previous studies that examined the strength of red shales in Ohio and West Virginia (Okagbue 1986 and Wu et al. 1987).

The XRD and Atterberg Limits results showed that the tested soil from US-231 is likely a degraded illite (as also discussed by Pomeroy and Thomas 1985).

The strength results were compared with existing correlations for both fully softened and residual strengths. These comparisons showed that the relationships implemented by Stark (2022) provided a reasonable fit for most of the soils if an uncertainty band of $\pm$5 degrees was considered for the secant friction angle. The exception to this was the residual strength for US-231, which was not well fit by any of the existing correlations. As the strength results from this study were consistent with previous results, it is believed that existing correlations for residual strength are not appropriate for use on degraded illite soils like those encountered at US-231. For sites with similar soils (red weathered shale or mudstone with LLs between 30 and 48 and PIs between 10 and 22), considering secant friction angles between 14 and 22 degrees is reasonable as a preliminary estimate, but site-specific testing should be performed to confirm these values are appropriate.

Slope stability analyses were performed for three of the sites (I-65, SR-5, and US-231). All three stability analyses used the strength envelopes measured in this study and demonstrated that these envelopes were consistent with observations (i.e., no movement at SR-5, limited movements at I-65, and a large failure at US-231). For SR-5, the use of a nonlinear envelope was critical to showing that this embankment had adequate stability. For US-231, the nonlinear envelope was able to demonstrate the slope would remain marginally stable under low water levels, while losing stability when the water table rose. The analyses using power envelopes were also able to show both a low factor of safety for the southbound lanes, which were the first to fail, and a larger marginally stable failure surface that reached beyond the northbound lanes. Once the southbound lanes began to move, they would have destabilized the entire surface leading to the larger failure. With the linear (secant) envelopes, the stability problems were either over or underpredicted and circular failure surfaces were not able to capture the larger movements. Noncircular surfaces were better able to capture the observed stability issues at I-65 due to the presence of a shallow limestone interval that served as a sliding plane in these analyses. Noncircular surfaces were not significantly different from the circular ones at US-231 or SR-5 and the differences at I-65 were not large enough to change the conclusion. Considering both circular and noncircular surfaces is considered to be good practice for stability analyses and requires minimal additional work with modern stability software and search algorithms.

6.2 Conclusions

Samples of clay collected at sites in west and north Alabama were characterized using index tests, geophysical measurements, and XRD. The results showed that the most common clay mineral is illite, with samples from I-65 in Conecuh County and SR-5 in Perry County showing larger proportions of montmorillonite. Clay samples from US-231 near Laceys Spring were unique in that the Atterberg Limits were similar to results collected at SR-219 in Bibb County, but the resistivity results were close to a sample from I-59 in Tuscaloosa County, which had a much higher LL and PI. XRD results showed that sample from US-231 is likely a degraded illite, which has been found in similar geologic units in eastern Ohio, western Pennsylvania and West Virginia. Degraded illites can classify as a low activity clay but have similar properties to montmorillonites (Fisher et al. 1968).

The saturated residual and fully softened strengths of the clays were measured over a wide range of stresses for all of the sites. Both linear and power envelopes were able to provide a similar fit to the data over a narrow stress range, but the power envelopes gave higher strengths at low stresses and lower strengths at higher stresses and were more consistent with the data across the full range of stresses. No tests were performed at stresses below 20 kPa, so it is not known how well either envelope represents the strengths at very shallow depths. The developed strength envelopes agree with previously developed correlations for soils with similar liquid limits, but a range of uncertainty ($\pm$5 degrees for the secant friction angle) should be considered.

The slope stability results demonstrated the importance of considering both the effects of suction and curved failure envelopes when examining the stability of slopes with high plasticity clays. For larger failures or sites with planar layering, noncircular surfaces should also be considered. Previous studies have shown that both the fully softened and residual strength envelopes are curved for these types of soils, but differences between these envelopes are often considered to be relatively minor and consideration of nonlinear envelopes is uncommon in practice. This study demonstrates that seemingly small differences in strength envelopes can have a significant effect on the factor of safety for shallow failure surfaces. Similarly, suction is known to increase strength, but is commonly neglected in slope stability analyses. This may be appropriate for initial design but realistic suction conditions should be considered for back analysis.

6.3 Recommendations for Implementation

The characterization results show that both Atterberg Limits and electrical resistivity can be good and complimentary tools to characterize the likely mineralogy of high and medium plasticity clays. The correlations between the mineralogy and the Atterberg Limits (Figure 3-1) were generally consistent with the XRD results and could be used to identify soils that are likely to be susceptible to strength loss. The lab and field based electrical resistivity measurements were able to show differences between the low strength sites like SR-5 and I-65 and the higher strength sites like SR-22 and SR-219, but the differences in resistivity may be hard to distinguish in the field and may be affected by other factors like water content and pore water chemistry. The results do show that sites with clay layers with resistivities below 5 ohm-m are likely to have significant strength loss. Electrical resistivity testing is recommended as a compliment to existing site characterization tools for landslide sites.

Ring shear testing was shown to be a reliable tool for determining both the fully softened and residual strengths. The test has the advantage of using disturbed samples, which allows testing to be performed on samples collected using any method (e.g., bulk samples, SPT, or tube). For sites, where estimates of drained strength parameters are critical to design, ring shear testing is recommended. For standard designs, the time and effort to prepare and test a ring shear sample may not be cost effective. For these sites, the fully softened and residual strength correlations implemented by Stark (2022) are recommended. These relationships showed a reasonable fit to the data from all sites with the exception of the residual strength at US-231 (discussed more below) as long as uncertainty in the estimates was considered. Using a range of $\pm$ 5 degrees for the secant friction angle appears to provide reasonable bounds, but this uncertainty range could be reduced through testing.

The slope stability analyses demonstrated that the measured strength envelopes produced results that were consistent with observations when nonlinear strength envelopes were used. For I-65, the difference between the linear and nonlinear envelopes was not significant as the linear envelope could be fit to the narrow range of effective stress conditions observed within the clay. For US-231 and SR-5, the use of the nonlinear power envelope improved agreement with the observations by capturing both the high secant friction angles at low stresses and the low secant friction angles at higher stresses. Power envelopes are included in most slope stability programs, including Slide and Slope/W (through the shear/normal function). If power envelopes are not

available secant friction angles should be fit at different stress levels and applied to the different regions of the model. Using a single linear fit may be adequate for sites without significant changes in effective stress, but the power fit eliminates the need to check for this.

One of the important conclusions from this study is the confirmation of the stability problems associated with the degraded illite clays within the Pennington formation. Similar soils have also caused landslide problems in Ohio, Pennsylvania, and West Virginia. These soils can be identified by screening for red or gray weathered shale or mudstone with LLs between 30 and 48 and PIs between 10 and 22 in deposits with either Mississippian or Pennsylvanian age rocks. Ring shear tests in this study showed that the strength envelope for the samples from US-231 shows more curvature in the residual strength envelope than would be expected for soils with those Atterberg Limits. This curvature leads to very low residual strengths that help explain the large failure observed at Laceys Spring. The current correlations for residual strengths do not adequately capture the strengths at this site and so a range of strengths (Figure 4-9) should be considered if similar soils are encountered at future sites.

REFERENCES

Advanced Geosciences Inc. (AGI), 2014, Earth Imager 2D Manual, Austin, TX.

ASTM D4318. (2018). Standard Test Methods for Liquid Limit, Plastic Limit, and Plasticity Index of Soils. ASTM International, West Conshohocken, PA.

ASTM D6467. (2013). Standard Test Method for Torsional Ring Shear Test to Determine Drained Residual Shear Strength of Cohesive Soils. ASTM International, West Conshohocken, PA.

ASTM D7928. (2017). Standard Test Method for Particle-Size Distribution (Gradation) of Fine-Grained Soils Using the Sedimentation (Hydrometer) Analysis. ASTM International, West Conshohocken, PA.

ASTM G57. (2020). Standard Test Method for Measurement of Soil Resistivity Using the Wenner Four-Electrode Method. ASTM International, West Conshohocken, PA.

Beaty, M. H. and Dickenson, S. E. (2015). Numerical Analysis for Seismically Induced Deformations in Strain-Softening Plastic Soils. *Proceeding 6th International Conference on Earthquake Geotechnical Engineering*, Christchurch, NZ.

Bowles, J. E. (1996). *Foundation Analysis and Design*. 5th ed. McGraw-Hill, Singapore.

Bromhead, E. N. (1979). A Simple Ring Shear Apparatus. *Ground Engineering, 12*, 40–44.

Chaudhary, B., Hazarika, H., and Krishan, A. M. (2016). Effect of Backfill Reinforcement on Retaining Wall Under Dynamic Loading. *Geotechnical Hazards from Large Earthquakes and Heavy Rainfalls*, 535–544.

Chen, C. Y., and Martin, G. R. (2002). Soil–structure Interaction for Landslide Stabilizing Piles. *Computers and Geotechnics*, *29*(5), 363–386.

Christensen, D. W., Bonaquist, R., and Jack, D. P. (2000). *Evaluation of Triaxial Strength as a Simple Test for Asphalt Concrete Rut Resistance*.

Constable, S.C., Parker, R.L. and Constable, C.G. (1987). Occam's inversion: A practical Algorithm for Generating Smooth Models from Electromagnetic Sounding Data. *Geophysics*, *52*, 289–300

Cook, M., Baker, R.M., Henderson, P., McGregor, S., and Moss, N. (2004). *Conecuh-Sepulga-Blackwater Rivers Watershed Protection Plan*. Alabama Geologic Survey: Tuscaloosa, AL.

Crabb, G. I., and Atkinson, J. H. (1991). Determination of Soil Strength Parameters for the Analysis of Highway Slope Failures. *Proceedings of the Slope Stability Engineering Developments and Applications: Proceedings of the International Conference on Slope*

Stability Organized by the Institution of Civil Engineers, Isle of Wight, 13–18.

Dawson, E. M., Roth, W. H., and Drescher, A. (1999). Slope Stability Analysis by Strength Reduction. *Géotechnique*, *49*(6), 835–840.

Degroot ‐ Hedlin, C., and Constable, S., (1990). Occam's Inversion to Generate Smooth, Two-Dimensional Models from Magnetotelluric Data. *Geophysics*, *55*(12), 1613–1624.

DeJong, J. T., Sturm, A. P., and Ghafghazi, M. (2016). Characterization of Gravelly Alluvium. *Soil Dynamics and Earthquake Engineering*, *91*, 104–115.

Duncan, J. M. (1996). State of the Art: Limit Equilibrium and Finite-Element Analysis of Slopes. *Journal of Geotechnical Engineering*, *122*(7), 577–596.

Duncan, J. M., Wright, S. G., and Brandon, T. L. (2014). *Soil Strength and Slope Stability*. John Wiley & Sons. Hoboken, N. J.

Dunkerley, D. L. (1976). A Study of Long-Term Slope Stability in the Sydney Basin, Australia. *Engineering Geology*, *10*(1), 1–12.

Eid, H. T., Rabie, K. H., and Wijewickreme, D. (2016). Drained Residual Shear Strength at Effective Normal Stresses Relevant to Soil Slope Stability Analyses. *Engineering Geology*, *204*, 94–107.

Eid, H. T., and Rabie, K. H. (2017). Fully Softened Shear Strength for Soil Slope Stability Analyses. *International Journal of Geomechanics*, *17*(1), 1–10.

Fisher, S. P., Fanaff, A. S., and Picking, L. W. (1968). Landslides of Southeastern Ohio. *The Ohio Journal of Science*, *68*(2), 65–80.

Fredlund, D. G., Morgenstern, N. R., and Widger, R. A. (1978). Shear Strength of Unsaturated Soils. *Canadian Geotechnical Journal*, *15*(3), 313–321.

Fredlund, D. G., Rahardjo, H. (1993). *Soil Mechanics for Unsaturated Soils*. John Wiley & Sons. Hoboken, N. J.

Fredlund, D. G. (2006). Unsaturated Soil Mechanics in Engineering Practice. *Journal of Geotechnical and Geoenvironmental Engineering*, *132*(3), 286–321.

Gao, L., Xia, J., Pan, Y., and Xu, Y. (2015). Reason and Condition for Mode Kissing in MASW Method. *Pure and Applied Geophysics*, *173*(5), 1627–1638.

Ghorbani, A., Jahanpour, R., and Hasanzadehshooiili, H. (2019). Evaluation of Liquefaction Potential of Marine Sandy Soil with Piles Considering Nonlinear Seismic Soil–Pile

Interaction; A Simple Predictive model. *Marine Georesources & Geotechnology*, *38*(1), 1–22.

Griffiths, D. V., and Lane, P. A. (1999). Slope stability analysis by finite elements. *Geotechnique*, 49(3), 387–403.

Gregersen, O. (1981). The Quick Clay Landslide in Rissa, Norway; The Sliding Process and Discussion of Failure Modes. *Proceedings International Conference on Soil Mechanics and Foundation Engineering*, *3*(10), 421–426.

Gunn, D. A., Chambers, J. E., Uhlemann, S., Wilkinson, P. B., Meldrum, P. I., Dijkstra, T. A., Haslam, E., Kirkham, M., Wragg, J., Holyoake, S., Hughes, P. N., Hen-Jones, R., and Glendinning, S. (2015). Moisture Monitoring in Clay Embankments Using Electrical Resistivity Tomography. *Construction and Building Materials*, *92*, 82–94.

Haefeli, R. (1951). Investigation and Measurements of the Shear Strengths of Saturated Cohesive Soils. *Géotechnique*, *2*(3), 186–208.

Heritage, R.J. (2013). Cyclic Softening Case Study: Wendover Retirement Village. *Proceeding 19th NZGS Geotechnical Symposium*, Christchurch, Queensland.

Hou, T., Xu, G., Shen, Y., Wu, Z., Zhang, N., and Wang, R. (2013). Formation Mechanism and Stability Analysis of The Houba Expansive Soil Landslide. *Engineering Geology*, *161*, 34–43.

Holtz, R. D. and Kovacs, W. D. (1981). *An Introduction to Geotechnical Engineering*. Prentice Hall, Englewood Cliffs, NJ, USA.

Holtz, R. D., Kovacs, W. D., and Sheahan, T. C. (2011). *An Introduction to Geotechnical Engineering*. Pearson, Upper Saddle River, NJ.

Jongmans, D., and Garambois S. (2007). Geophysical Investigation of Landslides: A Review. *Bulletin de la Société Géologique de France*, *178*(2), 101–112.

Jug, J., Stanko, D., Grabar, K., & Hrženjak, P. (2020). New approach in the application of seismic methods for assessing surface excavatability of sedimentary rocks. *Bulletin of Engineering Geology and the Environment*, *79*(7), 3797-3813.

Kennedy, L. (2019). Drained Residual Strength of Expansive Soils Causing Pavement Distress Along Alabama Highway 5. M.S. Thesis, Auburn University, Auburn, AL.

Khan, M. S., Hossain, S., Ahmed, A., and Faysal, M. (2017). Investigation of a Shallow Slope Failure on Expansive Clay in Texas. *Engineering Geology*, *219*, 118–129.

Kibria, G., and Hossain, S. (2017). Electrical Resistivity of Compacted Clay Minerals. *Environmental Geotechnics*, *6*(1), 18–25.

Kiernan, M. (2021). *Site Characterization and Modeling Considerations for Slopes Involving Fine Grained Strain-softening Soils*. Ph.D. Dissertation, Auburn University, Auburn, AL.

Kiernan, M., Jackson, D., Montgomery, J., Anderson, J. B., McDonald, B. W., and Davis, K. C. (2021). Characterization of a Karst Site using Electrical Resistivity Tomography and Seismic Full Waveform Inversion. *Journal of Environmental and Engineering Geophysics*, *26*(1), 1–11.

Knights, M. J., Montgomery, J., and Carcamo, P. S. (2020). Development of a Slope Failure Database for Alabama Highways. *Bulletin of Engineering Geology and the Environment*, *79*(1), 423–438.

Lade, P. V. (2010). The Mechanics of Surficial Failure in Soil Slopes. *Engineering Geology*, *114*(1–2),

Leong, E. C., and Abuel-Naga, H. (2018). Contribution of Osmotic Suction to Shear Strength of Unsaturated High Plasticity Silty Soil. *Geomechanics for Energy and the Environment*, *15*, 65–73.

L'Heureux Jean-Sébastien, Locat, A., Leroueil, S., Demers, D., and Locat, J. (2014). *Landslides in Sensitive Clays: From Geosciences to Risk Management*. Springer, Dordrecht.

Lin, C. P., Chang, C. C., and Chang, T. S. (2004). The Use of MASW Method in the Assessment of Soil Liquefaction Potential. *Soil Dyn. and Earthquake Engineering*, 24(9-10), 689–698.

Locat, A., Locat, P., Demers, D., Leroueil, S., Robitaille, D., and Lefebvre, G. (2017). The Saint-Jude Landslide of 10 May 2010, Quebec, Canada: Investigation and Characterization of the Landslide and its Failure Mechanism. *Canadian Geotechnical Journal*, 54(10), 1357–1374.

Loke, M. H. (2004). Tutorial: 2-D and 3-D Electrical Imaging Surveys: Geotomo Software. www.geoelectrical.com.

Lupini, J. F., Skinner, A. E., and Vaughan, P. R. (1981). Drained Residual Strength of Cohesive Soils. *Geotechnique*, *31*(2), 181–213.

Mesri, G., and Shahien, M. (2003). Residual Shear Strength Mobilized in First-Time Slope Failures. *Journal of Geotechnical and Geoenvironmental Engineering*, *129*(1), 12–31.

Mitchell, J. K., and Soga, K. (2005). *Fundamentals of Soil Behavior* (3rd ed.). John Wiley & Sons.

New York.

Mohammadi, S., and Taiebat, H. (2016). Finite Element Simulation of An Excavation-Triggered Landslide Using Large Deformation Theory. *Engineering Geology*, *205*, 62–72.

Montgomery, J. (2015). Issues in Nonlinear Deformation Analyses of Embankment Dams Affected by liquefaction. Ph.D. Dissertation, University of California, Davis.

Montgomery, J., Jackson, D., Kiernan, M., and Anderson, J. B. (2020). Use of Geophysical Methods for Sinkhole Exploration. Highway Research Center, *ALDOT Report 930–945*, Alabama Department of Transportation.

Montgomery, J., McDonald, B., Davis, K. C., Kiernan, M., and Jackson, D. (2021). Integrating Geophysics into Geotechnical Investigations along Alabama Highways. *FastTIMES*, v. 26, no. 2. Available online: https://fasttimesonline.co/integrating-geophysics-into-geotechnical-investigations-along-alabama-highways/

Montgomery, J., Kiernan, M., Jackson, D., and McDonald, B. (2022). Integrating surface-based geophysics into landslide investigations along highways. Proc., Geo-Congress 2022. ASCE, doi.org/10.1061/9780784484043.018

Nakamura, S., Wakai, A., Umemura, J., Sugimoto, H., and Takeshi, T. (2014). Earthquake Induced Landslides: Distribution, Motion and Mechanisms. *Soils and Foundations*, *54*(4), 544–559.

Okagbue, C. O. (1986). An Investigation of Landslide Problems in Spoil Piles in a Strip Coal Mining Area, West Virginia (U.S.A.). *Engineering Geology*, *22*(4), 317–333.

Park, C. B., Miller, R. D., and Xia, J. (1999). Multichannel analysis of Surface Waves. *Geophysics*, *64*(3), 800–808.

Park, C. B., and Miller, R. D. (2008). Roadside Passive Multichannel Analysis of Surface Waves (MASW). *Journal of Environmental and Engineering Geophysics*, *13*(1), 1–11.

Park, D.S. (2011). Strength loss and softening of sensitive clay slopes. Ph.D. Dissertation. University of California, Davis, CA, USA.

Perrone, A., Lapenna, V., and Piscitelli, S. (2014). Electrical Resistivity Tomography Technique for Landslide Investigation: A Review. *Earth-Science Reviews*, *135*, 65–82.

Pomeroy, J. S., Thomas, R. E. (1985). Geologic Relationships of Slope Movement in Northern Alabama. *U.S. Geological Survey Bulletin 1649*, United States Geologic Survey, Alexandria, VA.

Poppe, L. J., Paskevich, V. F., Hathaway, J. C., and Blackwood, D. S. A Laboratory Manual for X-Ray Powder Diffraction. *U.S. Geological Survey Open-File Report 01-041*. Woods Hole, MA, 2001

Reza Tabatabaiefar, S. H., Fatahi, B., and Samali, B. (2013). Seismic behavior of building frames considering dynamic soil-structure interaction. *International Journal of Geomechanics*, 13(4), 409–420.

Robertson, P. K. (1990). Soil Classification Using the Cone Penetration Test. *Canadian Geotechnical Journal*, *27*(1), 151–158.

Robertson, P. K. (2009). CPT Interpretation – A Unified Approach. *Canadian Geotechnical Journal*, *46*, 1-19.

Rocscience Inc. (2021). Slide 2 Version 9.013 - 2D Limit Equilibrium Analysis for Slopes. www.rocscience.com, Toronto, Ontario, Canada.

Russell, E. J., and Barker, R. D. (2010). Electrical Properties of Clay in Relation to Moisture Loss. *Near Surface Geophysics*, *8*(2), 173–180.

Schmertmann, J. (1978). Guidelines for CPT: Performance and Design. *Report FHWA-TS-78-209*, Federal Highway Administration, 145.

Schofield, A. N., Wroth, P. (1968). *Critical State Soil Mechanics*. McGraw-hill London, *310*.

Skempton, A. W. (1964). Long-Term Stability of Clay Slopes. *Géotechnique*, *14*, 77–102.

Skempton, A.W. (1970). First-Time Slides in Over-Consolidated Clays. *Géotechnique, 20*, 320–324.

Skempton, A. W. (1984). Slope Stability of Cuttings in Brown London Clay. *In Selected Papers on Soil Mechanics*. Thomas Telford Publishing, 241–250.

Skempton, A. W. (1985). Residual Strength of Clays in Landslides, Folded Strata and the Laboratory. *Géotechnique, 35*, 3–18.

Shannon, and Wilson. (1964). Report on Anchorage Area Soil Studies. *Rep. to USACE District, Anchorage, Alaska*. Contract no. DA-95-507-CIVENG-64-18.

Spencer, E. (1967). A method of Analysis of The Stability of Embankments Assuming Parallel Interslice Forces. *Géotechnique*, 17(1), 11–26.

Stallings, E. G. (2016). Investigation of Pavement and Subgrade Distress at Alabama Highway 5. M.S. Thesis, Auburn University, Auburn, AL.

Stark, T. D., Choi, H., and McCone, S. (2005). Drained Shear Strength Parameters for Analysis of

Landslides. *Journal of Geotechnical and Geoenvironmental Engineering*, *131*(5), 575–588.

Stark, T. D., and Eid, H. T. (1994). Drained Residual Strength of Cohesive Soils. *Journal of Geotechnical and Geoenvironmental Engineering*, *120*, 856–871.

Stark, T. D., and Eid, H. T. (1997). Slope Stability Analyses in Stiff Fissured Clays. *Journal of Geotechnical and Geoenvironmental Engineering*, *123*(4), 335–343.

Stark, T. D., and Fernandez, R. (2020). Fully Softened Shear Strength Measurement and Correlations. *Geotechnical Testing Journal*, *43*(5).

Stark, T. D., and Hussain, M. (2013). Empirical Correlations: Drained Shear Strength for Slope Stability Analyses. *Journal of Geotechnical and Geoenvironmental Engineering*, *139*(6), 853–862.

Stark, T. D., and Idries, A. (2021). Drained Residual Shear Strength Power Function Coefficients and b. *Geotechnical Testing Journal*, *44*(6).

Stark, T. D., and Vettel, J. J. (1992). Bromhead Ring Shear Test Procedure. *Geotechnical Testing Journal*, *15*(1), 24–32.

Stark, T.D. (2022) "Residual and Fully Softened Correlations Spreadsheet." Available from http://tstark.net/geotechnical-software. Last accessed on July 28, 2022.

Stephens, I., and Branch, A. (2013). Testing Procedure for Estimating Fully Softened Shear Strengths of Soils Using Reconstituted Material. Engineer Research and Development Center Vicksburg MS Geotechnical and Structures Lab: Vicksburg, MS.

Szabo, M. W. O., E.W., Copeland, C. W. Jr., Neathery, T. L. Geologic Map of Alabama, Geological Survey of Alabama Special Map 220, scale 1:250,000. 1988.

Taha, Mohd. R., Hossain, Md. K., and Mofiz, S. A. (2000). Effect of Suction on the Strength of Unsaturated Soil. *Proceedings of Advances in Unsaturated Geotechnics*, 210–221. Denver, Colorado.

Taipodia, J., Baglari, D., and Dey, A. (2018). Recommendations for Generating Dispersion Images of Optimal Resolution from Active MASW Survey. *Innovative Infrastructure Solutions*, *3*(1).

Thomspon, R. and Dapp, S. (2021). Innovative Landslide Solution. *Foundation Drilling.* April 2021.

Tiedemann, B. (1937). *Über die Schubfestigkeit bindiger Böden*; Preuß. Versuchsanst. f. Wasserbau u. Schiffbau.

Uhlemann, S., Hagedorn, S., Dashwood, B., Maurer, H., Gunn, D., Dijkstra, T., & Chambers, J. (2016). Landslide characterization using P-and S-wave seismic refraction tomography—The importance of elastic moduli. *Journal of Applied Geophysics*, *134*, 64-76.

Vandenberge, D. R., Duncan, J. M., and Brandon, T. L. (2013). Fully Softened Strength of Natural and Compacted Clays for Slope Stability. *In Proceedings of the Geo-Congress 2013: Stability and Performance of Slopes and Embankments III*, 221-233. San Diego, California.

Wathelet, M. (2005). Array Recordings Of Ambient Vibrations:Surface-Wave Inversion. Ph.D. Dissertation. Faculté des Sciences Appliquées, Liege University, Belgium.

Webb, J., David, K., and Collins, H. R. (1967). Geological Aspects of a Current Landslide in Vinton County, Ohio. *The Ohio Journal of Science*, *67*(2), 65–74.

Wright, S. G. (2005). Evaluation of Soil Shear Strengths for Slope and Retaining Wall Stability Analyses with Emphasis on High Plasticity Clays. *FHWA/TX-06/5-1874-01-1*. Federal Highway Administration: Washington, DC.

Wright, S. G., Zornberg, J. G., Aguettant, J. E. (2007). The Fully Softened Shear Strength of High Plasticity Clays. Center for Transportation Research, University of Texas, Austin, TX.

Wu, T. H., Williams, R. L., Lynch, J. E., & Kulatilake, P. H. (1987). Stability of slopes in red Conemaugh shale of Ohio. *Journal of geotechnical engineering*, *113*(3), 248-264.

Wu, T. H., Randolph, B. W., & Huang, C. S. (1993). Stability of shale embankments. *Journal of geotechnical engineering*, *119*(1), 127-146.

Xuan, M., Montgomery, J., and Anderson, J. B. (2021). Examining the effects of suction and nonlinear strength envelopes on the stability of a high plasticity clay slope. Geosciences. doi: 10.3390/geosciences11110449

Xuan, M. (2023). *Characterizing Strength Loss in Clays in Alabama*. Ph.D. Dissertation in preparation, Auburn University, Auburn, AL.

Yilmaz, I., and Karacan, E. (2002). A Landslide in Clayey Soils: An Example from the Kızıldag Region of the Sivas-Erzincan Highway (Sivas-Turkey). *Environmental Geosciences*, *9*(1), 35–42.

Yu, Y., Damians, I. P., and Bathurst, R. J. (2015). Influence of Choice of FLAC and PLAXIS Interface Models on Reinforced Soil–Structure Interactions. *Computers and Geotechnics*, *65*, 164–174.